Algorithm Theoretical Basis Document (ATBD)

for

GEDI Waveform Geolocation for L1 and L2 Products

Scott B Luthcke[1], Tim Rebold[2], Taylor Thomas[2], Teresa Pennington[3]

1. NASA Goddard Space Flight Center, Code 61A, Greenbelt, MD
2. Emergent Space Technologies, Laurel, MD
3. KBR Greenbelt, MD

Version 1.0
Release date: December 5th, 2019
Goddard Space Flight Center, Greenbelt, MD

Authors:

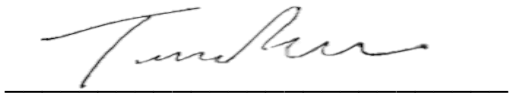

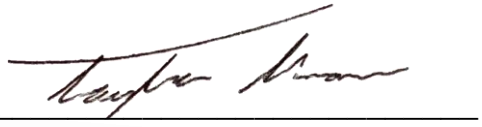

Principal Investigator:

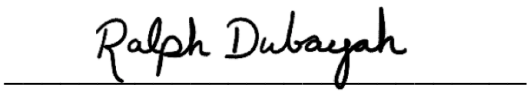

Abstract

The GEDI instrument consists of 3 lasers producing a total of 8 beam ground transects that are spaced approximately 600 m apart on the Earth's surface in the cross-track direction. Each beam transect consists of ~30 m footprint samples approximately spaced every 60 m along track. The "coverage" laser is split into two transects that are then each dithered producing four ground transects. The other two lasers are dithered only, producing two ground transects each. The fundamental footprint observations made by the GEDI instrument are received waveforms of energy (number of photons) as a function of receive time. By accounting for the speed of light, the GEDI waveforms are a distance measure of the vertical intercepted surfaces within a footprint. Captured within the receive footprint waveforms are the range to the ground and to various metrics of vegetation or "tree" height. The GEDI instrument precisely measures the time from transmit pulse of energy to any point within the receive waveform, and therefore, measures the round-trip time of the photons. Ranging points within the waveform that represent the lowest and highest points are computed in the L1A and L1B waveform processing. These ranging points are then geolocated, and therefore by simple interpolation, the geolocation for any other ranging point within the waveform can be easily computed for the higher level L2 products. The geolocation of the ranging points within each waveform is then provided in the geolocation group along with the geophysical corrections group for the Level 1 and Level 2 GEDI products.

The geolocation of a GEDI ranging point is computed as a function of three complex measurements: (1) the position of the space based ranging instrument from Precise Positioning (2) the pointing of the laser pulse from the Precise Pointing and (3) the waveform event round-trip travel time observation measured by the GEDI instrument. To transform these measurements into geolocated bounce points for each ranging point, a variety of models, algorithms, and corrections need to be adopted and applied. These include the determination of the instrument position and laser pointing within a consistent geodetic reference frame, the correction for atmospheric refraction path delay, ranging and time-tag corrections, the removal of unwanted geophysical effects such as tides, geoid and rotational deformation.

Foreword

This document is the Algorithm Theoretical Basis Document for the GEDI Waveform Geolocation for L1 and L2 Products. The GEDI Science Team and Science Operations Center team assumes responsibility for this document and updates it, as required, as algorithms are refined. Reviews of this document are performed when appropriate and as needed updates to this document are made.

This document is a GEDI ATBD controlled document. Changes to this document require prior approval of the project. Proposed changes shall be noted in the change log, as well as incrementing the document version number.

Questions or comments concerning this document should be addressed to:
Scott B. Luthcke
NASA Goddard Space Flight Center, Code 61A
Scott.B.Luthcke@nasa.gov
301-614-6112

Change History Log

Revision Level	Description of Change	Date Approved
1.0	Major revision to focus ATBD on geolocation congruent with the GEDI data products.	12/05/19

Table of Contents

List of Figures

List of Tables

1.0 INTRODUCTION

1.1 GEDI Data Products Overview

The GEDI Level 1 data products are developed in two separate products, a Level 1A (L1A) and a Level 1B (L1B) product. The GEDI L1A data product contains fundamental instrument engineering and housekeeping data as well as the raw waveform and geolocation information to compute higher level data products. The GEDI L1B geolocated waveform data product, while very similar to the L1A data product, contains specific data to support the computation of the higher level 2A and 2B data products. These L1B data include the corrected receive waveform, as well as the receive waveform geolocation information. The GEDI data products are noted below in Table 1-1.

Table 1-1 GEDI Data Products

Product	Description
Level 1	**Geolocated Waveforms**
Level 2	**Canopy Height/Profile Metrics** • **RH metrics** • **Canopy top height** • **Ground elevation** • **Canopy cover and cover profile** • **LAI and LAI profile**
Level 3	**Gridded Footprint Metrics**
Level 4	**Biomass**
Level 4	**Demonstrative Products** • Ecosystem model outputs • Enhanced height/biomass using fusion with Tandem X & Landsat • Habitat model outputs

1.2 Document Overview and Objective

This document is designed to provide an overview of the algorithms, methodology, and processing implementation required to compute the geolocation for each GEDI receive waveform and provide the geolocation information for the Level 1 and 2 data products. The geolocation data and information is provided within each of the L1 and L2 products under the "geolocation" and "geophys_corr" groups. The GEDI Waveform Processing ATBD provides an overview of the algorithms, methodology, and processing implementation required to compute the waveform ranging points, and the canopy height and profile metrics.

The ranges to the first and last bins of the receive waveform are used to compute the geolocation for any point within the waveform. Once the geolocation is evaluated for the two waveform

ranging points, the geolocation for any point within the waveform can be computed by simple linear interpolation between the two ranging points. The L1A and L1B data products contain the geolocation to the first and last bin ranging points. The L2A and L2B products contain the geolocation to specific points within the waveform computed by interpolating the geolocation of the two waveform ranging points.

The geolocation of a GEDI ranging point is computed as a function of three complex measurements: (1) the position of the space based ranging instrument from Precise Positioning (2) the pointing of the laser pulse from the Precise Pointing and (3) the waveform event round-trip travel time observation measured by the GEDI instrument. To transform these measurements into geolocated ranging points, a variety of models, algorithms, and corrections need to be adopted and applied. These include the determination of the instrument position and laser pointing within a consistent geodetic reference frame, the correction for atmospheric refraction path delay, ranging and time-tag corrections, and geophysical corrections such as ocean and solid earth tides and geoid.

1.3 GEDI Configuration

The GEDI instrument consists of three lasers producing a total of eight beam ground transects that are spaced approximately 600 m apart on the Earth's surface in the cross-track direction relative to the flight direction, and approximately 735 m of zonal (parallel to lines of latitude) spacing. Each beam transect consists of ~30 m footprint samples approximately spaced every 60 m along track. The "coverage" laser is split into two transects that are then each dithered producing four ground transects. The other two lasers are dithered only, producing two ground transects each. The configuration of the ground tracks is shown in Figure 1. The ranging points from each footprint's waveform are geolocated to produce geolocation data groups ("geolocation" and "geophys_corr") provided in the L1 and L2 data products.

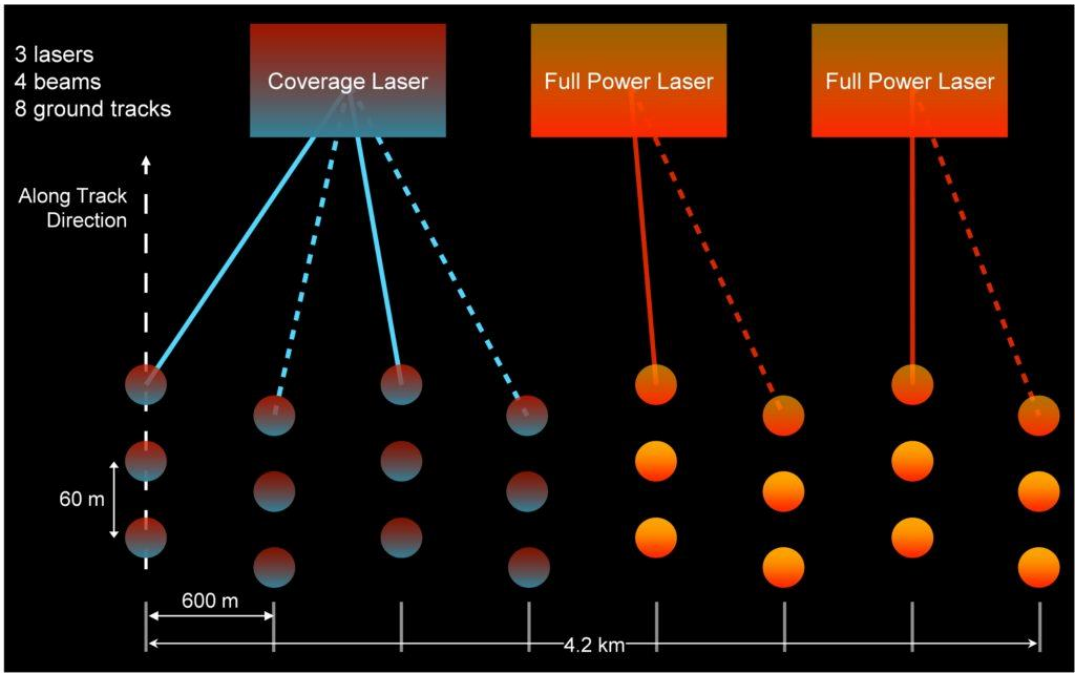

Figure 1 GEDI Beam Ground-track Configuration

1.4 Geolocation knowledge budget

Figure 2 presents the horizontal geolocation knowledge budget based on pre-launch assessment and assuming full system calibration. The full system calibration requires the analysis of many months of data to properly calibrate time varying biases. It is expected that early data products will likely not meet the geolocation knowledge budget presented in Figure 2.

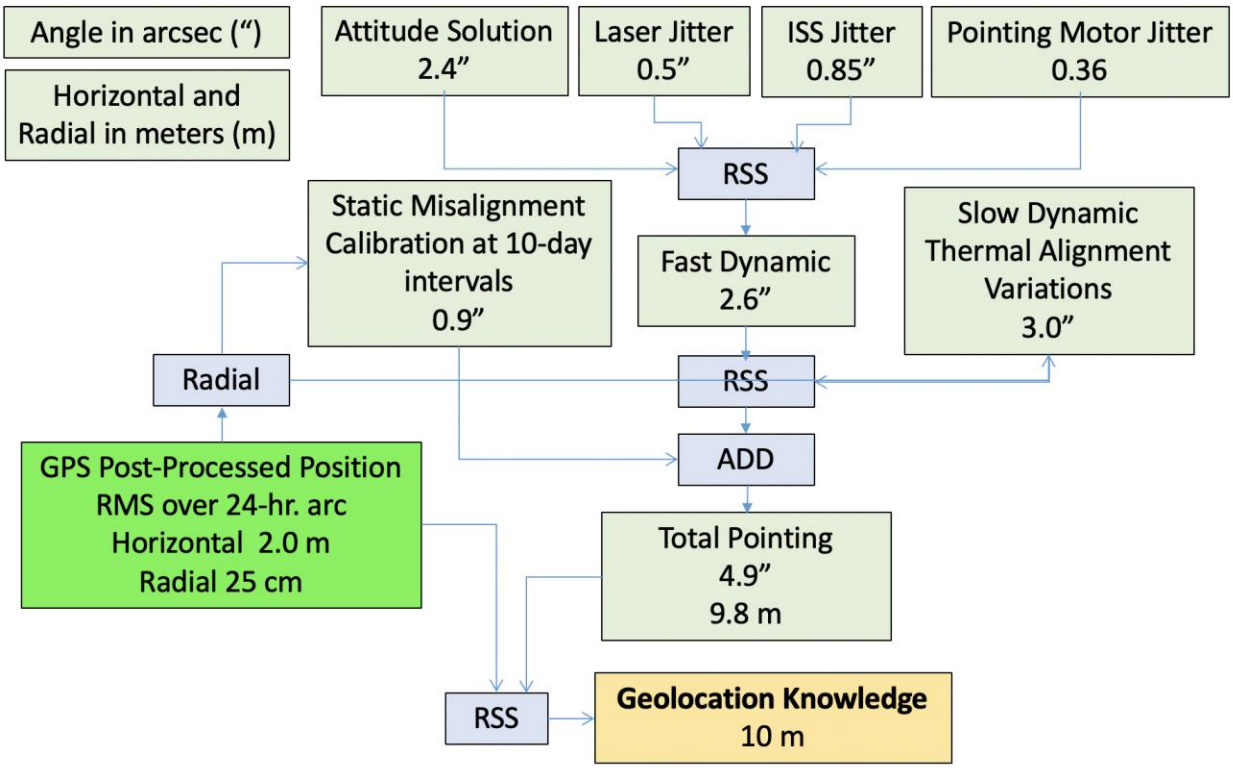

Figure 2 Horizontal Geolocation Knowledge Budget

1.5 Related Documentation

Related documents include parent documents and applicable documents, and information documents.

1.5.1 Parent Documents

- GEDI Science Data Management Plan

1.5.2 Applicable Documents

- GEDI ATBD for GEDI Transmit and Receive Waveform Processing for L1 and L2 Products.
- GEDI L1A Product Data Dictionary (gedi_l1a_product_data_dictionary.html)
- GEDI L1B Product Data Dictionary (gedi_l1b_product_data_dictionary.html)
- GEDI L2A Product Data Dictionary (gedi_l2a_product_data_dictionary.html)
- GEDI L2B Product Data Dictionary (gedi_l2b_product_data_dictionary.html)

The intention is for the GEDI mission geolocation to be in the same frame and to use consistent geophysical corrections as that of ICESat-2 in order to facilitate the direct comparison and use of these laser altimeter mission data. Additionally, in order to save effort and documentation, the GEDI mission directly references the following ICESat-2 ATBDs for documenting the geophysical corrections and the atmospheric path delay algorithms.

- ICESat-2 Project ATBD for Global Geolocated Photons, ATL03, Section 6.0 Geophysical Corrections.
- ICESat-2 Project ATBD for Atmospheric delay correction to laser altimeter ranges

2.0 GENERAL GEOLOCATION ALGORITHM

This section provides a generalized mathematical discussion of the rigorous geolocation for a spaceborne laser altimeter, properly computing the transmit range from the round-trip range. This covers the computation of the planet referenced location of the laser altimeter waveform ranging points where the instrument pointing, position, and observed range are known. The location of the ranging point (or also referred to in this document as a bounce point) can be commonly described in terms of geodetic latitude, longitude, and height above a reference ellipsoid or it can be represented in Cartesian coordinates in an Earth Centered Inertial (ECI) or Earth Centered Fixed (ECF) reference frame.

2.1 Reference Frames & Time Systems

Several reference frames are used in the precise positioning and precise pointing required for geolocation of GEDI footprints. The Space Station Analysis Coordinate System **(**SSACS) and GEDI frame are used to orient instruments relative to one another. The OBF provides a connection to the GEDI frame and a reference system for targeting calculations. Star tracker frames connect these to the ECI frame allowing conversion to geodetic coordinates. These frames are each described in the subsections below.

2.1.1 Space Station Analysis Coordinate System (SSACS).

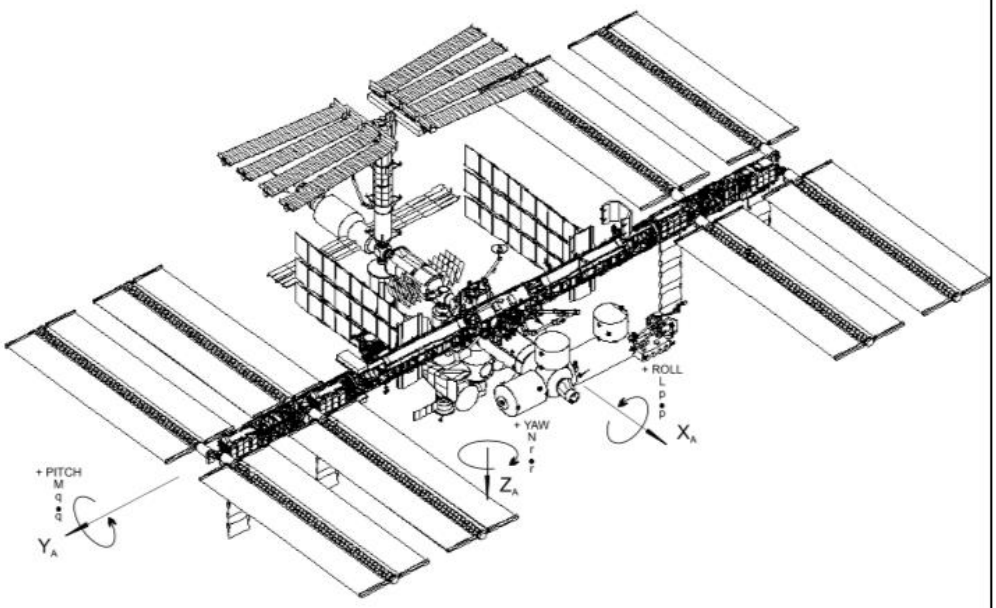

NAME:	Space Station Analysis Coordinate System
TYPE:	Right–Handed Cartesian, Body–Fixed
DESCRIPTION:	This coordinate system is derived using the Local Vertical Local Horizontal (LVLH) flight orientation. When defining the relationship between this coordinate system and another, the Euler angle sequence to be used is a yaw, pitch, roll sequence around the Z_A, Y_A, and X_A axes, respectively.
ORIGIN:	The origin is located at the geometric center of Integrated Truss Segment (ITS) S0 and is coincident with the S0 Coordinate frame. See figure 5.0–12, S0 coordinate frame for a more detailed description of the S0 geometric center.
ORIENTATION:	X_A The X–axis is parallel to the longitudinal axis of the module cluster. The positive X–axis is in the forward direction. Y_A The Y axis is identical with the S_O axis. The nominal alpha joint rotational axis is parallel with Y_A. The positive Y–axis is in the starboard direction. Z_A The positive Z–axis is in the direction of nadir and completes the right–handed Cartesian system. L, M, N: Moments about X_A, Y_A, and Z_A axes, respectively. p, q, r: Body rates about X_A, Y_A, and Z_A axes, respectively. $\dot{p}$, $\dot{q}$, $\dot{r}$: Angular body acceleration about X_A, Y_A, and Z_A axes, respectively.
SUBSCRIPT:	A

Figure 3 Space Station Analysis Coordinate System (SSACS) Definition. (From: "The Space Station Reference Coordinate Systems document, Figure 4.0-1")

2.1.2 GEDI Frame (GED)

The GEDI frame (GED) is used to locate all the key instrument sub-systems (GPS, star trackers, instrument tracking points) and mechanical interfaces for the GEDI payload. The GEDI Coordinate System has its origin in the interface plane of the Payload Interface Unit (PIU) and the GEDI payload on the centerline. The +X-axis is normal to the PIU interface plane and extends along the centerline in the positive direction away from the PIU (which is typically opposite to the ISS orbital velocity). The +Z-axis is in the interface plane and extends in the positive direction away from the grappling fixture (typically in the Nadir direction). The +Y-axis completes the right-hand orthogonal system (typically in the port direction).

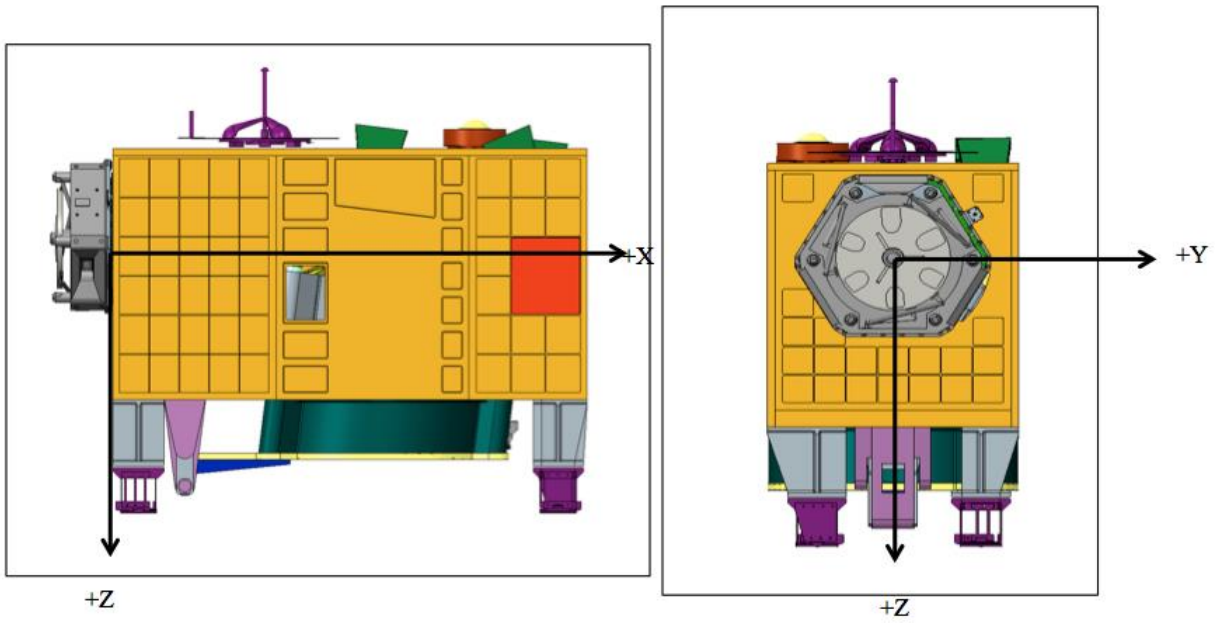

Figure 4 GEDI Frame (GED) Orientation

2.1.3 Optical Bench Frame (OBF)

The Optical Bench frame is used to specify the GEDI beam pointing vectors and serves as the reference coordinate system for performing targeting computations (following the reference ground track). The origin of the OBF frame is the center of the pinhole circle center of the telescope assembly (on the optical axis of the telescope). The X-Y plane is parallel to the Optical Bench on the side of the Optical Bench that holds the telescope. The +Z-axis is aligned with the telescope bore sight, normal to the optical bench and defines the pointing direction for PCS. The OBF +X and +Y-axes are nominally aligned with the GED +X and +Y-axes, respectively.

The optical bench is rotated relative to GED about the Y-axis (pitch) to counter negative ISS pitch bias. Let the angle of this rotation be θ. For $\theta > 0$, the rotation tends to move the +Z axis *towards* the ISS orbital velocity; this is the preferred direction to counter an ISS pitch bias (which would tend to rotate GED +Z *away* from the ISS orbital velocity.
The transformation between GED and OBF is

$$R_{GED\rightarrow OBF} = \begin{bmatrix} \cos(\theta) & 0 & -\sin(\theta) \\ 0 & 1 & 0 \\ \sin(\theta) & 0 & \cos(\theta) \end{bmatrix} \quad (2.1.3.1)$$

GED is not used for precise calculations but, rather, intended to be descriptive with respect to electronics boxes and structure. The tilt angle θ is measured only coarsely and *GED to OBF* does not need an associated misalignment correction matrix.

2.1.4 Star Tracker Frames (ST1, ST2 and ST3)

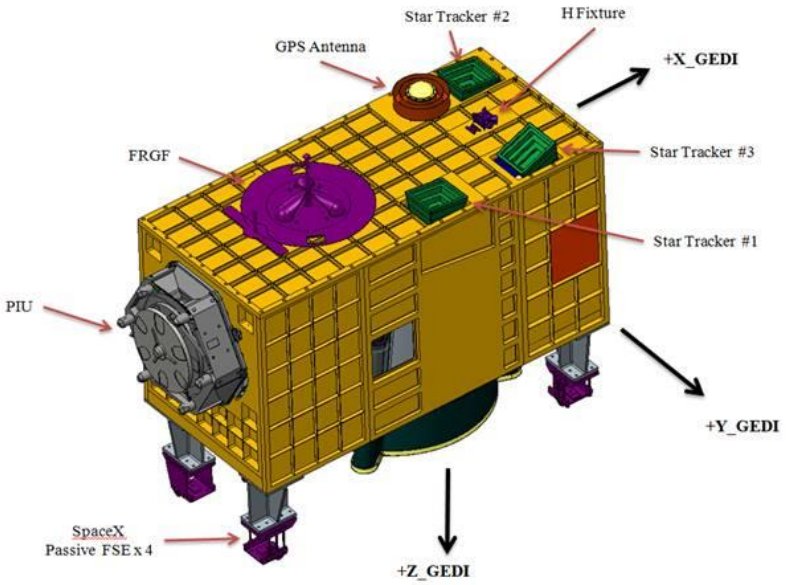

Figure 5 Star Tracker Locations

The star tracker system for GEDI contains 3 camera head units (CHU) with baffle, and a central data processing unit (DPU) manufactured by the Danish Technical University (DTU). The optical field of view (FOV) of each of the CHU's is 18.4ºx13.4º, full angle. The GEDI star trackers are located on the outward face of the optical bench, approximately at the vertices of an isosceles right triangle of short sides 0.5 m (See Figure 5). The boresights are approximately anti-aligned with the optical telescope.

Each CHU has an intrinsic reference frame defined by DTU as having an origin at the intersection of the CCD plane with the optical axis of the camera. The camera +Z-axis points along the boresight towards the stars being imaged, the +X-axis is in the CCD plane along the long side of the CCD and points towards the data harness, and the +Y-axis completes the right-handed triad (see Figure 6). The three frames are labeled ST1, ST2, and ST3. The attitude solution from each CHU is output as a quaternion that defines ECI-to-ST1, ECI-to-ST2, or ECI-to-ST3.

The CHU assemblies will be equipped with reference cubes that allow the orientations of the star tracker frames to be established on the optical bench. Table 2-1 provides the bore-sight alignments of each CHU relative to OBF.

Table 2-1 Star Tracker Bore Sight Alignments With Respect to OBF. Entries are Rotation Angles in Degrees

CHU No.	Cant Y (degrees forward/aft)	Cant X (degrees port/starboard)
1	0	0
2	0	2 (starboard)
3	-30 (forward)	0

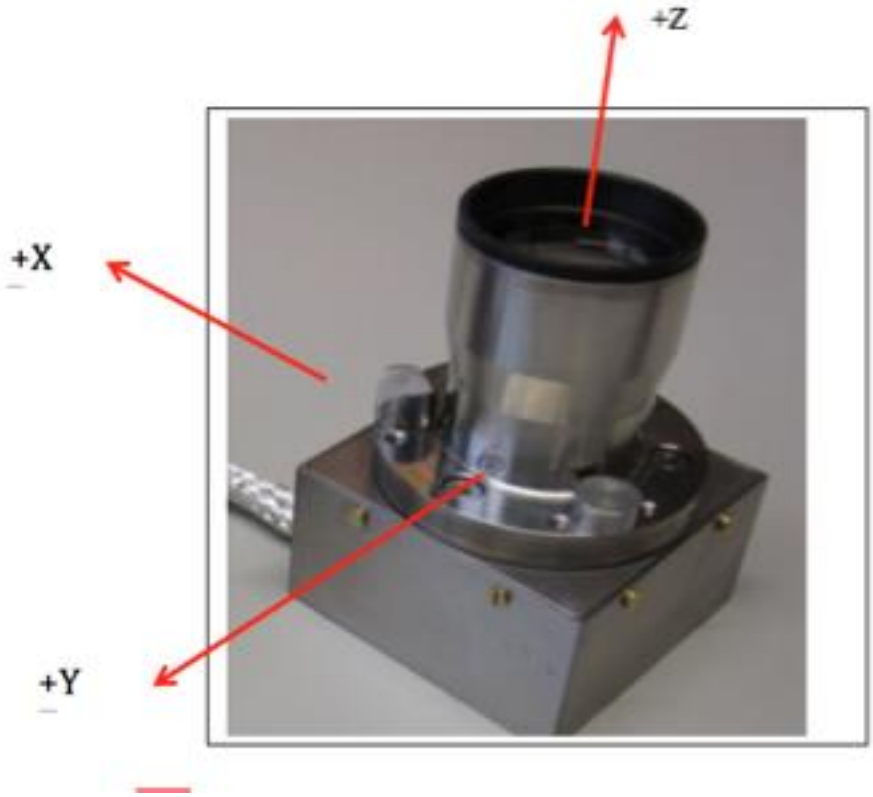

Figure 6 µASC CHU/µIRU With Illustration of the CHU Reference Frame

The rotation matrices are computed as:

$$R_{ST\#\rightarrow OBF} \equiv RotZ * RotY * RotX$$
$$= \begin{pmatrix} CZ & SZ & 0 \\ -SZ & CZ & 0 \\ 0 & 0 & 1 \end{pmatrix} \begin{pmatrix} CY & 0 & -SY \\ 0 & 1 & 0 \\ SY & 0 & CY \end{pmatrix} \begin{pmatrix} 1 & 0 & 0 \\ 0 & CX & SX \\ 0 & -SX & CX \end{pmatrix} \begin{pmatrix} 1 & 0 & 0 \\ 0 & -1 & 0 \\ 0 & 0 & -1 \end{pmatrix} \quad (2.1.4.1)$$

where *CX* and *SX* are the cosine and sine, respectively, of the port/starboard cant angle and *CY* and *SY* are the cosine and sine, respectively, of the forward/aft cant angle. Rotation about Z is nominally zero. The right-most factor represents a 180-degree rotation about X (to account for the opposite directions of STA Z and OBF Z). Absent any cant, the rotation about the star tracker X-axis is 180 degrees.

The three rotation matrices from the respective star tracker frames to the OBF are as follows:

$$R_{ST1\rightarrow OBF} = MA1\begin{pmatrix}1 & 0 & 0\\ 0 & -1 & 0\\ 0 & 0 & -1\end{pmatrix} \quad (2.1.4.2)$$

$$R_{ST2\rightarrow OBF} = MA2\begin{pmatrix}1.000 & 0 & 0\\ 0 & -0.9994 & -0.0349\\ 0 & 0.0349 & -0.9994\end{pmatrix} \quad (2.1.4.3)$$

$$R_{ST3\rightarrow OBF} = MA3\begin{pmatrix}0.8660 & 0 & -0.5000\\ 0 & -1 & 0\\ -0.5000 & 0 & -0.8660\end{pmatrix} \quad (2.1.4.4)$$

Here *MA1*, *MA2*, and *MA3* are misalignment factors, nominally set to the 3×3 identity matrix, that are based on on-orbit calibration of the telescope-to-star tracker camera alignment.

2.1.5 ECF to ECI

The current ECI frame employed for the GEDI altimeter measurement modeling and geolocation is the geocentric realization of the International Celestial Reference System (ICRS), namely the ICRF Geocentric mean equator and equinox of 2000 Jan 1.5 (J2000.0) defined by the International Earth Rotation Service (IERS), and realized by use of the JPL Development Ephemeris DE403, and the Lunar Ephemeris LE403 [Standish et al., 1995 & *Petit and Luzum, 2010*].

The geodetic reference frame, which is consistently used in the analysis of altimeter data, is the International Terrestrial Reference Frame (ITRF). The ITRF definition and other current modeling recommendations of the IERS are documented in the "IERS Conventions" [*Petit and Luzum, 2010*].

Transformation between the ICRF and the ITRF is accomplished using the following equation:

$$[ICRF] = P(t)N(t)R(t)W(t)[ITRF] \qquad (2.1.5.1)$$

where

$P(t) = precession\ transformation$

$N(t) = nutation\ transformation$

$R(t) = sidereal\ rotation\ transformation$

$W(t) = polar\ motion\ transformation$

The precession – nutation transformations follows IAU 2000 [*Cappola et al., 2009*]. The rotation transformation is just a rotation around the Earth's spin axis by $-\theta_g$, where θ_g is the Greenwich True Sidereal Time at epoch *t*. The *R(t)* and *W(t)* transformations are described in [*Petit and Luzum, 2010*].

2.1.6 Time systems, Time Tagging, and Laser Shot Round-Trip Timing

The integration of the satellite equations of motion requires a uniform time system. The system used in the POD processing software, GEODYN, is the Terrestrial Dynamic Time (TDT) (also referred to as Terrestrial Time (TT)) [*Guinot, 1991, McCarthy, 1996*]. The TDT time is in practice determined from the International Atomic Time (TAI):

$$TDT = TAI + 32.184\ s \qquad (2.1.6.1)$$

The TDT time must be converted to the conventional time scales used by most observers for time-tagging satellite observations and tracking data. The conventional time scales relevant to most laser altimeter missions are UTC and GPS time.

UTC, or Coordinated Universal Time, is an atomic time system which runs at the same rate as TAI, but is periodically adjusted by one second steps in order to keep it near the UT1 time system. The UT1 time system is the non-uniform time determined by observations of the stars from the non-uniformly rotating Earth, after correcting for polar motion. Correction factors relating UTC and UT1, and UTC and TAI, are provided by the IERS Bulletin B or by the USNO Rapid Service (IERS Bulletin A).

GPS Time [*Hofmann-Wellenhof et al., 1994*] is the time system to which all GPS clocks and observables are referenced. It is also an atomic time system derived from TAI. GPS Time can be computed from:

$$GPS = TAI - 19.000\ s \qquad (2.1.6.2)$$

Calendar dates are referenced to the Julian Date (JD) or the Modified Julian Date (MJD) [*Taff, 1985*]. The current standard epoch is J2000.0 which is JD = 2451545.0, or January 1.5, 2000.

The GPS system uses the GPS standard epoch of JD = 2444244.5 or January 6.0, 1980. An important unit for the GPS system is the GPS week, which is defined as:

$$GPS\ week = INT\ [(JD - 2444244.5) / 7] \qquad (2.1.6.3)$$

where INT[x] is the largest integer smaller than x.

The GEDI data time tag is provided as a Master Time with an integer part and a fractional part. This Master Time represents the number of seconds from the GEDI Master Time Epoch, and is derived from the GEDI instrument Oven Controlled Oscillator (OCXO) clock counting from each GPS receiver one pulse per second (1PPS). The GPSR 1PPS includes a time stamp that has the precise date and time for the 1PPS within 50 nanoseconds when the GPSR is operational and clock steering (the nominal mode). Therefore, using the GEDI OCXO counting from each 1PPS allows each GEDI laser shot to be precisely time tagged. The Master Time is also provided in the data products as delta_time.

The data products provide the GEDI Master Time Epoch in the ancillary data group. The below is the GEDI Master Time Epoch nominally used, but the user is strongly encouraged to extract this parameter value from the data product. GEDI Master Time Epoch is the number of seconds from the GPS Epoch 1980-01-06T00:00:00Z to the GEDI Epoch 2018-01-01T00:00:00Z. Therefore, to compute the time of a GEDI laser shot, the Master Time (or delta seconds from the GEDI epoch) is added to the GEDI Master Time Epoch to obtain the time in GPS seconds from the GPS Epoch. The GPS seconds can then be transformed to any other time system .

In addition, the OCXO is used to compute the round-trip time of the laser pulse which provides the precise ranging for geolocation. The OCXO performance over short-time intervals is better than 24 parts per billion, allowing for ranging precision below 2 cm per shot. Furthermore, the OCXO is continuously calibrated by integrating the number of cycles of the OCXO between GPSR 1PPS, and therefore, estimating the OCXO delta frequency correction at each calibration window. Nominally, the calibration window is 30 seconds, and typically results in a calibration of the OCXO frequency at the few parts per billion level resulting in sub-cm ranging precision.

2.2 Generalized Input

Each beam the laser transmits is time tagged with respect to GPS time. Ranging points are computed from the received waveform as part of the L1A process. The lowest and highest points from the received waveform are computed and then geolocation can be derived for any points between these two points by interpolation. The following procedure pertains to geolocating any receive ranging point given its associated transmit time tag.
The geolocation of a ranging point (again also referred to as a bounce point) utilizes the following input:

- The round-trip range observed by the instrument, 2o, given by

$$2 \cdot o = c\Delta t \quad (2.2.1)$$

$$\Delta t = T_R - T_T \quad (2.2.2)$$

  Where
  c is the speed of light
  T_R is the receive time of the ranging point
  T_T is the transmit time of the laser pulse

- The pulse transmit time and receive time are easily related:

$$T_T = T_R - \frac{2 \cdot o}{c} \quad (2.2.3)$$

- Position and Velocity of the instrument reference point in the ECI frame at T_T

$$\vec{X}^{\,T}_{IRP},\ \vec{V}^{\,T}_{IRP} \quad (2.2.4)$$

- Instrument attitude described as the rotation from the GEDI coordinate system (GED) to ECI at T_T

$$R^T_{GED \to ECI} \quad (2.2.5)$$

- Laser altimeter pointing described as a unit vector in the ECI frame at T_T

$$\hat{u} = R^T_{OBF \to ECI} \hat{L}^T_{OBF} \quad (2.2.6)$$

  Where
  $R^T_{OBF \to ECI}$ is the rotation from the Optical Bench Frame (OBF) to the ECI frame at T_T
  $\hat{L}^T_{OBF}$ are the laser beam unit vectors in the OBF frame at T_T

- The pointing vector is then modified to take into account the instrument velocity in ECI (velocity aberration).

$$\hat{p} = \frac{c\hat{u} + \vec{V}^T_{IRP}}{|c\hat{u} + \vec{V}^T_{IRP}|} \quad (2.2.7)$$

- Instrument transmit and receive tracking point offsets, referenced from the instrument reference point in the ECI frame at T_T and T_R respectively:

$$\vec{x}^T_{off} = R^T_{GED \to ECI}[\vec{s}^T_{TTP} - \vec{s}^T_{IRP}] \quad (2.2.8)$$

$$\vec{x}^R_{off} = R^R_{GED \to ECI}[\vec{s}^T_{RTP} - \vec{s}^R_{IRP}] \quad (2.2.9)$$

  Where

$\vec{s}^{T}_{IRP}$, $\vec{s}^{R}_{IRP}$ is the instrument reference point vector in the GED frame at T_T
$\vec{s}^{T}_{TTP}$ is the instrument transmit tracking point in the GED frame at T_T
$\vec{s}^{T}_{RTP}$ is the instrument receive tracking point in the GED frame at T_R

Note that all the vectors given in 2.2.8 and 2.2.9 are referenced to constant origin coordinates in the GED reference frame.

2.3 Preliminary Computations

Given the above, the computation of the receive ranging point location follows.

- In order to compute the location of the ranging or bounce point it is necessary to know the path delay due to atmospheric refraction. However, in order to compute the path delay, the bounce point location is needed. Computing the path delay at an approximate bounce point location solves this problem. The midpoint of the observed two-way range (o) corrected for range biases is used as the approximate location. The error incurred is less than 1 m at 5° off-pointing, which is sufficient to compute the atmospheric refraction delay to sub-mm accuracy (1 m in height is roughly 0.25 mm in path delay).

  Approximate bounce point location for atmospheric refraction delay computation:

$$\vec{X}^{B}_{BPapprox} = \vec{X}^{T}_{IRP} + \vec{x}^{T}_{off} + \rho \cdot \hat{p} \qquad \rho = o - o_{Ibias} \quad (2.3.1)$$

  Where

  o_{Ibias} is the one-way instrument range bias

- Given the above, the atmospheric refraction model can be evaluated for the bounce point in question and a range correction can be computed (see ICESat-2 Project ATBD for Atmospheric delay correction to laser altimeter ranges).

  The corrected one-way observation is then computed:

$$\rho_{corr} = \rho - \Delta\rho_{atmref} \quad (2.3.2)$$

  Where

  ρ_{corr} is the corrected one-way range observation
  $\Delta\rho_{atmref}$ is the atmospheric refraction path delay

- Now, the receive time is computed using the observed range corrected for instrument biases:

$$T_R = T_T + \frac{2\rho}{c} \quad (2.3.3)$$

The instrument reference point, in the ECI frame, is then computed at T_R

$$\vec{X}^{R}_{IRP} \quad (2.3.4)$$

2.4 Light Time Solution for Bounce Point

The altimeter measures a round-trip (two-way) range from the transmitted laser pulse to the Earth and back again to the detector. During this round-trip (~2.8 ms for GEDI) the instrument position changes appreciably. The effect of this change in position causes the two legs of the altimeter

round-trip to be unequal. Therefore, we rigorously reconstruct the entire path of the two-way range. This enables the accurate computation of both the time tag of the bounce point and the one-way range from the instrument at transmit time to the bounce point, which is necessary for the geolocation computation. The following outlines this procedure:

- Consider a triangle formed by each leg of the round-trip range and the line connecting the instrument transmit and receive tracking points at T_T and T_R. Using the law of cosines we can write an expression for the total round-trip range as a function of the transmit leg range. Then an iterative procedure is used to solve for a scale factor which, when multiplied by one half the corrected observation, gives the transmit range.

$$|\vec{x}^R|^2 = |\vec{x}^{TR}|^2 + |\vec{x}^T|^2 - 2(\vec{x}^{TR} \cdot \vec{x}^T) \quad (2.4.1)$$
$$\vec{x}^T = \rho_{corr}^T \cdot \hat{p} \quad (2.3.2)$$
$$\vec{x}^{TR} = \left[\vec{X}_{IRP}^R + \vec{x}_{off}^R\right] - \left[\vec{X}_{\mathrm{IRP}}^T + \vec{x}_{off}^T\right] \quad (2.4.3)$$

- Now, the round-trip corrected observation can be expressed as:

$$\rho_{corr}^T + \rho_{corr}^R = \rho_{corr}^T + [|\vec{x}^{TR}|^2 + (\rho_{corr}^T)^2 - 2\rho_{corr}^T(\vec{x}^{TR} \cdot \hat{p})]^{\frac{1}{2}} \quad (2.4.4)$$

- The total round-trip corrected range is expressed with the corrected one-way range multiplied by a scale factor:

$$\rho_{corr}^T = s\rho_{corr} \quad (2.4.5)$$
$$Total(s) = s\rho_{corr} + [|\vec{x}^{TR}|^2 + (s\rho_{corr})^2 - 2s\rho_{corr}(\vec{x}^{TR} \cdot \hat{p})]^{\frac{1}{2}} \quad (2.4.6)$$

- Therefore, the corrected transmit leg range may be computed by estimating *s*.
  The iterative procedure below is performed to estimate *s*:
  1. First iteration, $i = 1$ and guess $s(1) = 1$
  2. Evaluate $\varepsilon(i)$:
     $$\varepsilon(1) = 2\rho_{corr} - Total(s(1)) \quad (2.4.7)$$
  3. Evaluate $\varepsilon(i), for\ i = 2$ and guess $s(2) = 0.99$
  4. Compute gradient ∇f
     $$\nabla f = \frac{(\varepsilon(i) - \varepsilon(i-1))}{(s(i) - s(i-1))} \quad (2.4.8)$$
  5. Update *s:*
     $$s(i+1) = s(i) + \Delta s(i), \quad \Delta s(i) = \frac{-\varepsilon(i)}{\nabla f} \quad (2.4.9)$$
  6. If $\varepsilon(i+1) \leq 1mm$, then the solution has converged, otherwise repeat steps 4-6
  7. After convergence the transmit leg range is: $\rho_{corr}^T = s'\rho_{corr}$ (2.4.10)

2.5 Computation of Bounce Point Location in ECI and Time Tag

The bounce point ECI location and time tag are necessary to compute the location of the bounce point in the Earth Centered Fixed frame (ECF), and to correct this bounce point for time varying effects such as Earth tides, ocean tides, and ocean loading.

- The bounce point location in ECI can be rigorously computed using the converged transmit leg range computed above:

$$\vec{X}^{B}_{B(ECI)} = \vec{X}^{T}_{IRP} + \vec{x}^{T}_{off} + s'\rho_{corr} \cdot \hat{\rho} \quad (2.5.1)$$

- The bounce point time must be computed with the uncorrected transmit leg range:

$$T_B = T_T + s' \frac{\rho}{c} \quad (2.5.2)$$

2.6 Computation of ECF Time Specific Bounce Point Location

- The ECI bounce point position is then rotated to ECF coordinates using the rotations due to precession (P), nutation (N), the Earth's spin (R) and polar motion (W) at the bounce point time (see Section A.1, Reference Frames, for details):

$$\vec{X}^{B}_{B(ECF)} = W(T_B)R(T_B)N(T_B)P(T_B)\vec{X}^{B}_{B(ECI)} \quad (2.6.1)$$

- Once the ECF bounce point position is computed the time varying surface displacement effects (e.g. solid Earth and ocean tides) at T_B can be evaluated and removed (reference ICESat-2 Project ATBD for Global Geolocated Photons, ATL03, Section 6.0 Geophysical Corrections).

2.7 Computation of Geodetic Coordinates

Finally, it is desired to represent the location of the bounce point in a spherical coordinate system defined by an ellipsoid of revolution representing the general geometric shape of the Earth. The ECF bounce point position is then transformed to geodetic coordinates of latitude, longitude and height above the reference ellipsoid. The algorithm can be found in Section 3.2.

3.0 GEDI IMPLEMENTATION

In this section the specific details of the GEDI implementation are presented. These details include the specific input and output products, time systems and reference frame details, as well as approximations to both simplify computations and to better facilitate post-geolocation analysis and correction.

3.1 Approximate Geolocation Algorithm

Section 2 presented a mathematical treatment for the rigorous geolocation of a receive ranging point. This treatment included the light time solution where the transmit range is specifically computed from the round-trip range measured by the altimeter instrument. In addition, the algorithm corrected the range for atmospheric path delay before the final steps of the geolocation. In the following GEDI implementation the geolocation is performed with an approximate algorithm which negates the need to compute the transmit range from the round-trip range for the purposes of geolocation only (not for altimeter measurement modeling for instrument calibration). What follows is a step-by-step algorithm for geolocating the receive ranging points. The input parameters for the geolocation algorithm are defined in Table 3.1. The sources of the input parameters are defined in the last column. The calculated L1A and L1B output parameters from the geolocation algorithm are defined in Table 3.2.

Table 3-1 Input Parameters for the GEDI Geolocation Algorithm

Value	Units	Description	Variable	Source
For Section 3.1 Approximate Geolocation Algorithm				
Shot Number		Unique shot identifier with orbit and beam number information	*shot_number*	L1A *shot_number*
Round-trip times to top and bottom of waveform.	m	2-way range for first and last bin waveform ranging points, converted from bins to meters using the OCXO calibrated frequency and speed of light	Δt	L1A *range_bin0_m* and *range_lastbin_m*
Laser transmit time for receive ranging observations	sec	Transmit pulse start time in GPS time	t_T	L1A *delta_time*
range bias	m	Computed Instrument cal/val analysis ranging biases per beam	o_{bias}	ANC04 and provided in L1A *range_bias_correction*
one-way average range	m	one-way range corrected for the range bias and atmospheric path delay	ρ	Calculated
Speed of light	m/sec	Constant	c	Table 4-8
GEDI instrument reference point	m	Provided in OBF frame	$\vec{s}_{IRP}$	ANC04

Value	Units	Description	Variable	Source
For Section 3.1 Approximate Geolocation Algorithm				
Instrument transmit and receive tracking point	m	Instrument transmit tracking points given in OBF frame	$\vec{s}_{TTP}$	ANC04
OBF to ECI Frame quaternions		OBF to ECI quaternions	$R_{OBF \rightarrow ECI}$	ANC05
GEDI GPS antenna reference point position and velocity	m, m/sec	Computed at bounce time by interpolating the precise positioning output	$\vec{X}_{IRP}, \vec{V}_{IRP}$	ANC04
Pointing unit vector in inertial frame (ECI)	Unit vector	Calibrated for each beam	$\hat{L}_{ECI}$	ANC05
Pointing unit vector in Optical Bench Frame (OBF)	Unit vector	Calibrated for each beam	$\hat{L}_{OBF}$	ANC05
ECI to ECF quaternions		Interpolated from ECI to ECF daily quaternions	$R_{ECI \rightarrow ECF}$	ANC03
For Section 3.2 Computing geodetic spherical coordinates referenced to the ellipsoid from ECF Cartesian Coordinates				
Semi-major axis	m	Semi-major axis of the adopted Earth ellipsoid (Section 3.2)	a_e	Table 4-8
Semi-minor axis	m	Semi-minor axis of the adopted Earth ellipsoid (Section 3.2)	b_e	Table 4-8
Flattening		Flattening of the adopted Earth ellipsoid (Section 3.2)	f	Table 4-8

Table 3-2 Calculated Output Parameters for GEDI Geolocation Algorithm

Algorithm: only needed internally for the algorithm per receive ranging point group **/geolocation: the geolocation output parameters to be retained in the /geolocation group in L1 and L2 products**				
Value	**Units**	**Description**	**Variable**	**Target Output**
Laser transmit time for receive ranging observations	sec	Transmit pulse start time in GPS time	t_T	/geolocation group in L1 and L2 products *delta_time*
Corrected receive times for all receive ranging points in the group	sec	Calculated from the first and last bin waveform ranging point transmit time and observed round-trip range corrected for range bias	t_R	Algorithm

Algorithm: only needed internally for the algorithm per receive ranging point group **/geolocation: the geolocation output parameters to be retained in the /geolocation group in L1 and L2 products**				
Value	**Units**	**Description**	**Variable**	**Target Output**
Bounce point times for the receive waveform ranging points	sec	Calculated from the first and last bin ranging point transmit time and the one-way range corrected for range bias	t_B	/geolocation *bounce_time_offset_bin0* *bounce_time_offset_lastbin*
Instrument transmit tracking point offset in ECI	m	Calculated at transmit time from instrument tracking point and reference point vectors in OBF frame and transformed using OBF to ECI rotation	$\vec{x}_{off}$	Algorithm
Transmit pointing vector in ECI	Unit vector	Computed at transmit time	$\hat{p}$	Algorithm
Atmospheric path delay	m	Calculated using the atmospheric path delay algorithm for receive waveform ranging points	ρ_{atm}	/geolocation *neutat_delay_total_bin0* *neutat_delay_total_lastbin*
Atmospheric path delay derivative with respect to ellipsoid height	m/m	Calculated using the atmospheric path delay algorithm for receive waveform ranging points	$\frac{\partial \rho_{atm}(j)}{\partial h(j)}$	/geolocation *neutat_delay_derivative_bin0* *neutat_delay_derivative_lastbin*
Bounce point locations in ECI	m	Bounce point locations in ECI computed for the first and last bin waveform ranging points. Includes range bias and atmospheric path delay corrections to range.	$\vec{B}_{ECI}$	Algorithm
Bounce point locations in ECF	m	Inertial bounce point locations rotated to ECF by interpolating the ECI to ECF quaternions. Includes geophysical corrections (see Section 3.7)	$\vec{B}_{ECF}$	Algorithm
Geodetic latitude of bounce points	radians	Computed from ECF first and last bin waveform ranging point positions.	ϕ	/geolocation *latitude_bin0* *latitude_lastbin*
East longitude of bounce points	radians	Computed from ECF first and last bin waveform ranging point positions.	λ	/geolocation *longitude_bin0* *longitude_lastbin*

Algorithm: only needed internally for the algorithm per receive ranging point group **/geolocation: the geolocation output parameters to be retained in the /geolocation group in L1 and L2 products**				
Value	**Units**	**Description**	**Variable**	**Target Output**
Ellipsoid height of bounce points	m	Computed from ECF first and last bin waveform ranging point positions. Includes geophysical corrections (see Section 3.7)	h	/geolocation *elevation_bin0* *elevation_lastbin*
Unit pointing vector in ECF	Unit vector	Unit pointing vector in ECF for the waveform ranging points	$\hat{u}(j)$	Algorithm
Azimuth of the unit pointing vector	radians	Azimuth of the unit pointing vector for the waveform ranging points in the local ENU frame in radians. The angle is measured from North and positive towards East.	$Az(j)$	/geolocation *local_beam_azimuth*
Elevation of the unit pointing vector	radians	Elevation of the unit pointing vector for the receive waveform ranging points in the local ENU frame in radians. The angle is measured from East-North plane and positive towards Up.	$El(j)$	/geolocation *local_beam_elevation*

Table 3-3 Geolocation Error Input and Output Parameters

Input: Needed to compute geolocation error uncertainty **Output: Geolocation output error uncertainties computed in Section 3.6**				
Value	**Units**	**Description**	**Variable**	**Target / Source**
Position 1-σ error estimate	m	1-σ position uncertainty estimates in inertial frame	$\delta\vec{X}^{\sigma}_{ECI}$	ANC04
Range 1-σ error estimate	s	1-σ uncertainty in receive waveform ranging points average one-way range	δo^{σ}	L1A *range_bin0_error* *range_lastbin_error*
Pointing 1-σ error estimate	radians	1-σ uncertainty quaternion of the laser pointing	δq^{σ}_{L}	ANC05
Geodetic latitude 1-σ error estimate	degree	Geodetic latitude 1-σ uncertainty of the reference ranging point	$\Delta\phi(j)$	/geolocation *latitude_bin0_error* *latitude_lastbin_error*
East longitude 1-σ error estimate	degree	East longitude 1-σ uncertainty of the reference ranging point	$\Delta\lambda(j)$	/geolocation *longitude_bin0_error* *longitude_lastbin_error*
Ellipsoid height 1-σ error estimate	m	Ellipsoid height 1-σ uncertainty of the reference ranging point	$\Delta h(j)$	/geolocation *elevation_bin0_error* *elevation_lastbin_error*

The following ancillary data products support the geolocation computations.

Table 3-4 ANC Product Files

Product File	**Description**
ANC03	ECI to ECF Quaternions
ANC04	Precise Positioning Determination Ephemeris
ANC05	Precise Pointing Determination Vectors and Quaternions

STEP 1: Range Observations and Time Tags

For each laser shot the L1A data provides the transmit time of the laser shot and the round-trip time to a ranging point "*i*" (e.g. bin0 or last bin of the waveform). A one-way average range corrected for range bias is computed next. The instrument range bias is obtained from the instrument team's ground calibration as *a priori* and the science team's instrument calibration analysis post-launch. It is important to note that these corrections will be dependent on the beam, so each beam will have its own individual range bias information.

$$for\ a\ ranging\ point\ "i"\ L1A\ gives \qquad t_T(i), \Delta t(i) \qquad (3.1.1)$$

$$\rho(i) = \frac{c\,\Delta t(i)}{2} + o_{bias} \qquad (3.1.2)$$

Corrected receive time is then computed:

$$t_R(i) = t_T(i) + \frac{2\rho(i)}{c} \qquad (3.1.3)$$

The approximate bounce point time is computed:

$$t_B(i) = t_T(i) + \frac{\rho(i)}{c} \qquad (3.1.4)$$

STEP 2: Instrument Transmit Tracking Point Vector in the ECI Frame

The vector from the instrument reference point to the transmit tracking point is computed at transmit time in the OBF frame and then rotated to the ECI frame. The instrument reference point in the OBF frame is assumed to be fixed in time and is equivalent to the GPS antenna reference point given in Section 4, Precise Positioning.

The OBF to ECI rotation is computed from the interpolation of the ECI to OBF quaternions. See Section 3.5 concerning a note about interpolation.

$$\vec{x}_{\,off}(i) = R_{OBF\rightarrow ECI}\big(t_T(i)\big)\big[\vec{s}_{TTP}\big(t_T(i)\big) - \vec{s}_{IRP}\big(t_T(i)\big)\big] \qquad (3.1.5)$$

STEP 3: Instrument Reference Point Position and Velocity in the ECI Frame

The instrument reference point ECI position and velocity are computed at the bounce time by interpolating the daily ANC04 Precise Positioning output. See Section 3.5 concerning a note about interpolation.

$$\vec{X}_{\,IRP}\,\big(t_B(i)\big), \qquad \vec{V}_{IRP}\,\big(t_B(i)\big) \qquad (3.1.6)$$

STEP 4: Transmit Pointing Vector in ECI Frame

The ECI laser beam pointing unit vector is computed at transmit time interpolating the following data set for each beam:

ANC05 – pointing unit vector in ECI frame calibrated for each beam

$$\hat{p}(i) = \hat{L}_{ECI}\big(t_T(i)\big) \qquad (3.1.7a)$$

Alternatively, the data set created in ANC05 is a product of the calibrated beam unit vectors expressed in the OBF frame and transformed using the ECI to OBF quaternions.

$$\hat{p}(i) = R'_{ECI \to OBF}\left(t_T(i)\right)\hat{L}_{OBF}\left(t_T(i)\right) \quad (3.1.7b)$$

Where $R'_{ECI \to OBF} = R_{OBF \to ECI}$

STEP 5: Bounce Point ECI Cartesian Coordinates

As noted in Section 2.3, in order to compute the location of the ranging or bounce point it is necessary to know the path delay due to atmospheric refraction. However, in order to compute the path delay, the bounce point location is needed. Computing the path delay at an approximate bounce point location solves this problem. The one-way range corrected for range bias is used to compute the approximate bounce location. The error incurred is less than 1 m at 5° off-pointing, which is sufficient to compute the atmospheric refraction delay to sub-mm accuracy (1 m in height is roughly 0.25 mm in path delay).

The approximate bounce point ECI Cartesian coordinates are computed as follows:

$$\vec{B}_{ECI\_approx}(i) = \vec{X}_{IRP}\left(t_B(i)\right) + \vec{x}_{off}(i) + \rho(i) \cdot \hat{p}(i) \quad (3.1.8)$$

Given the above, the atmospheric refraction model can be evaluated for the approximate bounce point and a range correction can be computed (see ICESat-2 Project ATBD for Atmospheric delay correction to laser altimeter ranges).

The corrected one-way range is then computed:

$$\rho_{corr} = \rho - \rho_{atm} \quad (3.1.9)$$

Where

ρ_{corr} is the corrected one-way range observation

ρ_{atm} is the atmospheric refraction path delay

The bounce point ECI Cartesian coordinates can then be computed as follows:

$$\vec{B}_{ECI}(i) = \vec{X}_{IRP}\left(t_B(i)\right) + \vec{x}_{off}(i) + \rho_{corr}\,(i) \cdot \hat{p}(i) \quad (3.1.10)$$

STEP 6: Bounce Point ECF Cartesian Coordinates

The bounce point ECI Cartesian coordinates are then rotated to ECF by interpolating the daily ECI to ECF quaternions in product ANC03:

$$\vec{B}_{ECF}(i) = R_{ECI \to ECF}\left(t_B(i)\right)\vec{B}_{ECI}(i) \quad (3.1.11)$$

Equation 3.1.10 is an approximation to the geolocation algorithm presented in Section 2 which performs the light time solution to compute the transmit range. Equation 3.1.10 uses the instrument transmit tracking point and pointing vector evaluated at transmit time as in the rigorous geolocation algorithm. However, equation 3.1.10 uses the instrument reference point position evaluated at the bounce time as well as the average one-way range instead of the true transmit leg range. It should also be noted that velocity aberration is not applied as in the rigorous geolocation algorithm. The maximum ISS motion is approximately 2.7 cm in altitude and approximately 10.8 m along-track over one-way shot travel time or approximately 1.4 milliseconds. The total position change of the ISS from transmit time to bounce time compensates for the range difference between the simple one-way range and actual transmit leg range, and provides the along-track shift equivalent to

velocity aberration. This approximate geolocation algorithm has been shown to be accurate to a few tenths of a millimeter in total bounce point position during nominal reference ground track mapping and 5° off-point calibration maneuvers. While this approximation serves the purposes of receive ranging point geolocation well, the rigorous light time solution of the transmit leg range is employed in the direct altimetry and dynamic crossover measurement modeling used for instrument parameter calibration from altimeter range residual analysis (see Section 6, *Instrument Calibration and Parameter Estimation*).

The bounce point is also corrected for several geophysical corrections (see Section 3.7).

STEP 7: Bounce Point Latitude, Longitude and Height Computation
The ECF bounce points computed in 3.1.11 are then converted to a geodetic spherical coordinate system relative to the reference ellipsoid using the algorithm defined in Section 3.2.

Input to the Section 3.2 algorithm: the array of ECF bounce points for *N* ranging points: $\vec{B}_{ECF}(i)$
Output from the Section 3.2 algorithm: the following arrays for *N* ranging points:

$\phi(i)$ is the geodetic latitude, the acute angle between the semi-major axis and a line through the observer perpendicular to the spheroid
$\lambda(i)$ is the east longitude, the angle measured eastward in the equatorial plane between the Greenwich meridian and the observer's meridian
$h(i)$ is the ellipsoid height, the perpendicular height above the reference ellipsoid
*Note: WGS84 ellipsoid parameters are used and are defined in Section 4.3.3 Table 4-8.

Note: Section 3.4 provides the algorithm to apply a new atmospheric range correction entirely in geodetic spherical coordinates referenced to the ellipsoid without going back to the ECI or ECF frames or requiring re-computation of the position and pointing vectors.

3.2 Computing Geodetic Spherical Coordinates Referenced to the Ellipsoid from ECF Cartesian Coordinates

Assumption: h << N, e<<1
The ECF bounce point Cartesian coordinates are converted to geodetic coordinates of latitude, longitude and height above the reference ellipsoid. The reference ellipsoid of the Earth can be uniquely defined by:

$a_e -$ semimajor axis of the Earth reference ellipsoid
$b_e -$ semiminor axis of the Earth reference ellipsoid
$f = \dfrac{a_e - b_e}{a_e}$ – flattening factor of the Earth reference ellipsoid (3.2.1)
$e^2 = 1 - (1 - f)^2 -$ Earth eccentricity squared (3.2.2)

The following geodetic coordinates are then computed from the reference ellipsoid:

ϕ is the geodetic latitude, the acute angle between the semi-major axis and a line through the observer perpendicular to the ellipsoid
λ is the east longitude, the angle measured eastward in the equatorial plane between the Greenwich meridian and the observer's meridian

h is the ellipsoid height, the perpendicular height above the reference ellipsoid

The geodetic coordinates are computed from the ECF Cartesian coordinates of the bounce point using the following iterative procedure:

- ECF Cartesian coordinates of the bounce point are expanded in the below equations to be X, Y, Z.
- Make initial estimate for parameter *t:*

$$t \cong e^2 Z \quad (3.2.3)$$

- Compute the following quantities on each iteration:

$$Z_t = Z + t \quad (3.2.4)$$

$$(N + h) = \sqrt{X^2 + Y^2 + Z_t^2} \quad (3.2.5)$$

$$sin\phi = \frac{Z_t}{(\mathrm{N} + \mathrm{h})} \quad (3.2.6)$$

$$N = \frac{a_e}{\sqrt{1 - e^2\, sin^2\phi}} \quad (3.2.7)$$

$$t = Ne^2 sin\phi \quad (3.2.8)$$

- When t converges (sub-mm), the ellipsoid height is the difference of the bounce point distance from the center of curvature and the surface distance from the center of curvature. This is given by:

$$h = (N + h) - N \quad (3.2.9)$$

- Geodetic latitude and longitude are then given by:

$$\phi = tan^{-1}\left(\frac{Z_t}{\sqrt{X^2 + Y^2}}\right) \text{ or } sin^{-1}\left(\frac{Z_t}{(N + h)}\right) \quad (3.2.10)$$

$$\lambda = \tan^{-1}\left(\frac{Y}{X}\right) \quad (3.2.11)$$

3.3 Computing Azimuth and Elevation in the Local ENU Frame

Given geodetic latitude and longitude coordinates *(ϕ, λ),* a unit vector in Earth Centered Fixed coordinates (x, y, z) can be expressed as a unit vector in local East-North-Up (ENU) coordinates (E, N, U):

$$\begin{bmatrix} u_E \\ u_N \\ u_U \end{bmatrix} = \begin{bmatrix} -sin\lambda & cos\lambda & 0 \\ -cos\lambda sin\phi & -sin\lambda sin\phi & cos\phi \\ cos\lambda cos\phi & sin\lambda cos\phi & sin\phi \end{bmatrix} \begin{bmatrix} u_x \\ u_y \\ u_z \end{bmatrix} \quad (3.3.1)$$

Azimuth and elevation are given by:

$$El = \sin^{-1}(u_U), \quad -90° \leq El \leq 90° \quad (3.3.2)$$

$$Az = \mathrm{atan2}(u_E, u_N), \quad -180° \leq Az \leq 180° \quad (3.3.3)$$

3.4 Applying a New Atmospheric Range Correction in Geodetic Spherical Coordinates Referenced to the Ellipsoid.

Given the geodetic spherical coordinates for ranging bounce points that already have the correction for atmospheric path delay included, as well as the ENU azimuth, elevation, original atmospheric path delay and the derivative of the path delay with respect to ellipsoid height:

$$\phi'(i), \quad \lambda'(i), \quad h'(i)$$
$$Az(i), \quad El(i), \quad \rho_{atm}(i), \quad \frac{\partial \rho_{atm}(i)}{\partial h(i)}$$

We can compute new geodetic lat, lon and height for the ranging bounce points given a new atmospheric path delay. The new atmospheric path delay and derivative are computed for the reference ranging bounce point:

$$\rho_{Natm}(i), \quad \frac{\partial \rho_{Natm}(i)}{\partial h(i)}$$

The delta atmospheric path delay is then computed:

$$\Delta\rho_{atm}(i) = \left(\rho_{Natm}(i) - \rho_{atm}(i)\right) \quad (3.4.3)$$

Where the original bounce point height is used to evaluate the new atmospheric path delay. The original path delay was computed at the approximate bounce point which is not retained in the data product, and the new path delay is computed from the original geolocated bounce point. Any differences in the bounce point locations used in evaluating the atmospheric path delay result in small errors, as 1 m in height is roughly 0.25 mm in path delay. The /geolocation group also contains the partial derivative of the path delay with respect to ellipsoid height to further evaluate and correct the computation if necessary.

Compute the earth radius at the bounce points using the parameters of the reference ellipsoid:

$$R_E(i) = \sqrt{\frac{(a_E^2 \cos(\phi'(i)))^2 + (b_E^2 \sin(\phi'(i)))^2}{(a_E \cos(\phi'(i)))^2 + (b_E \sin(\phi'(i)))^2}} \quad (3.4.4)$$

Compute the pointing unit vector in the ENU frame from *Az* and *El* for the reference ranging point:

$$\begin{bmatrix} u_E \\ u_N \\ u_U \end{bmatrix} = \begin{bmatrix} \cos El(j) \sin Az(j) \\ \cos El(j) \cos Az(j) \\ \sin El(j) \end{bmatrix} \quad (3.4.5)$$

This pointing vector is used in the computation for all ranging points in the group. The change in latitude due to the change in the atmospheric path delay correction can be expressed in radians as:

$$\Delta\phi(i) = \frac{-\Delta\rho_{atm}(i) u_N}{R_E} \quad (3.4.6)$$

The change in longitude due to the change in the atmospheric path delay correction can be expressed in radians as:

$$\Delta\lambda(\mathrm{i}) = \frac{-\Delta\rho_{atm}(i)u_E}{R_E \cos\phi} \quad (3.4.7)$$

The change in height due to the change in the atmospheric path delay correction can be expressed in meters as:

$$\Delta h(i) = -\Delta\rho_{atm}u_U \quad (3.4.8)$$

Compute new latitude, longitude and height due to the difference between the new and original atmospheric path delay:

$$\phi^N(i) = \phi'^{(i)} + \Delta\phi(i) \quad (3.4.9)$$
$$\lambda^N(i) = \lambda'^{(i)} + \Delta\lambda(i) \quad (3.4.10)$$
$$h^N(i) = h'^{(i)} + \Delta h(i) \quad (3.4.11)$$

3.5 A Note about Position, Velocity and Quaternion Interpolation

A Hermite 9th or 10th order polynomial interpolation algorithm is recommended for interpolating the spacecraft position and velocity data. The Hermite interpolator has been shown to be both extremely computationally efficient and extremely accurate to sub-micron and sub-micron/s when interpolating a typical LEO ephemeris with 5 – 30 second data postings. The Hermite interpolator naturally provides interpolation of both position and velocity. It is recommended that the algorithm implementer perform a thorough evaluation of the interpolation performance before implementing operationally.

A Lagrange 9th order polynomial interpolation has been found to be accurate to 0.002" when interpolating a time series of quaternions with 5 second sampling. It is recommended that the algorithm implementers use this interpolator as a baseline, but should perform a thorough validation.

3.6 Geolocation Output Parameter Error Computation

This section discusses how uncertainties in the geolocation inputs affect the expected geolocation accuracy. The input and output parameters in Table 3-3 are used and computed respectively for the reference ranging point *i* for each group of ranging points. For any reference ranging point there are three primary inputs that are essential for geolocation. These inputs are a product of the orbit and pointing determination of the instrument, and the timing of the ranging measurement. They are shown below,

$$\left(\vec{X}_{ECI}, \hat{p}, \rho\right)$$

These inputs produce a ranging bounce point location $\vec{B}_{ECI}$ in the inertial frame.

$$\vec{B}_{ECI} = \vec{X}_{ECI} + \rho \cdot \hat{p}$$

The term $\vec{X}_{ECI}$ is the inertial position of the instrument transmit tracking point. The term $\hat{p}$ is the pointing vector transformed into the inertial frame and corrected for velocity aberration (rigorous formulation), and ρ is the transmit range corrected for instrument biases and path delay (Rigorous formulation: Section 2, Equation 2.4.10; Approximate Formulation: Section 3, Equation 3.1.2).

Geolocation errors are computed as the difference between the observed ranging bounce point position computed with input errors ε, and the true ranging bounce point position computed without input errors,

$$\Delta\vec{B}_{ECI} = \vec{B}_{ECI}^{\,observed} - \vec{B}_{ECI}^{\,truth}$$

The errors on the input parameters represent a perturbed state $x_0 + \Delta x$, that is perturbed by Δx from reference state x_0. A Taylor series expansion about this reference state yields,

$$\vec{B}_{ECI}(x_0 + \Delta x) = \vec{B}_{ECI}(x_0) + \left.\frac{\partial \vec{B}_{ECI}}{\partial x}\right|_{x_0} \Delta x + hot$$

Higher order terms hot are neglected in this study. The parameter x represents the inputs that are under study in this analysis. The geolocation errors can be rewritten in terms of the input parameters as,

$$\Delta\vec{B}_{ECI} = \vec{B}_{ECI}(x_0 + \Delta x) - \vec{B}_{ECI}(x_0), \qquad \Delta x = \varepsilon$$

The input errors are assumed to have zero-mean and be represented adequately by diagonal covariance matrix *P*,

$$\varepsilon \sim N(0, P), \qquad P = \begin{bmatrix} \sigma_x^2 & 0 & 0 \\ 0 & \sigma_y^2 & 0 \\ 0 & 0 & \sigma_z^2 \end{bmatrix}$$

The inertial geolocation errors can be transformed into the radial, in-track and cross-track (RIC) frame for an easier understanding of the error distribution,

$$\Delta\vec{B}_{RIC} = R_{ECI\to RIC}\Delta\vec{B}_{ECI}$$

- **Computing Radial, In-track and Cross-track Components (RIC)**

Given position $\vec{R}_{ECI}$ and velocity $\vec{V}_{ECI}$ vectors in a chosen reference frame (ECI) the transformation matrix from that chosen frame into radial, in-track and cross-track components can be expressed as,

$$\hat{z} = \frac{\vec{R}_{ECI}}{\left|\vec{R}_{ECI}\right|} = [z_1\ z_2\ z_3]$$

$$\hat{y} = \frac{\hat{z} \times \vec{V}_{ECI}}{\left|\hat{z} \times \vec{V}_{ECI}\right|} = [y_1\ y_2\ y_3]$$

$$\hat{x} = \frac{\hat{y} \times \hat{z}}{|\hat{y} \times \hat{z}|} = [x_1\ x_2\ x_3]$$

$$R_{ECI\to RIC} = \begin{bmatrix} z_1 & z_2 & z_3 \\ x_1 & x_2 & x_3 \\ y_1 & y_2 & y_3 \end{bmatrix}$$

$$\begin{bmatrix} u_{radial} \\ u_{intrack} \\ u_{cross} \end{bmatrix} = R_{ECI \to RIC} \begin{bmatrix} u_x \\ u_y \\ u_z \end{bmatrix}$$

where u is any vector expressed in the chosen frame in which the position and velocity vectors were provided. For the geolocation error analysis the inertial instrument reference point position and velocity interpolated to the reference ranging point j's bounce point time, $\vec{X}_{IRP}\left(t_B(j)\right)$ and $\vec{V}_{IRP}\left(t_B(j)\right)$ respectively are used to compute this reference frame.

- **Rigorous and Approximate Geolocation Algorithm Notes**

The rigorous and approximate geolocation algorithms were shown to agree to within tenths of a millimeter (Section 3, Equation 3.1.11) in total bounce point position during nominal reference ground track mapping and 5° scan maneuvers. In the following sections, we present the rigorous formulation to show how the exact relation between the geolocation inputs and outputs. In the end we present the relationships using the inputs from the approximate algorithm. Keep in mind that the approximate algorithm introduces additional error into the geolocation output, but that its magnitude is negligible and can be ignored. The most notable differences between the two algorithms are the approximation of the bounce point time and transmit range magnitude. The approximate algorithm uses the instrument position interpolated at the approximate bounce point time. Using the bounce point time accounts for velocity aberration and eliminates the need to use the spacecraft velocity to modify the pointing. The approximate algorithm also assumes that both transmit and receive ranges are equal in length. All of these simplifications produce nearly the same result as the rigorous formulation. Extensive testing was performed to validate the accuracy of the approximate algorithm and geolocation error output computations. We now present the theory of errors introduced into the geolocation output from uncertain input estimates.

- **Position Errors**

Input errors on the instrument inertial position are given by,

$$\vec{X}_{ECI}^{\,observed} = \vec{X}_{ECI}^{\,truth} + \varepsilon, \qquad \Delta\vec{X}_{ECI} = \vec{X}_{ECI}^{\,observed} - \vec{X}_{ECI}^{\,truth} = \varepsilon$$

These errors have mean and variance statistics of,

$$E\{\varepsilon\} = 0, \qquad E\left\{\varepsilon_j \varepsilon_j^T\right\} = \sigma_j^2$$

We start with the geolocation computation,

$$\vec{B}_{ECI} = \vec{X}_{ECI} + \rho \cdot \hat{p}$$

We form the geolocation errors as,

$$\Delta\vec{B}_{ECI} = \vec{B}_{ECI}^{\,observed} - \vec{B}_{ECI}^{\,truth} = \upsilon$$

$$\Delta\vec{B}_{ECI} = \left(\vec{X}_{ECI}^{\,observed} + \rho \cdot \hat{p}\right) - \left(\vec{X}_{ECI}^{\,truth} + \rho \cdot \hat{p}\right) = \varepsilon$$

The resulting geolocation errors υ are simply equal to the position errors and have the exact error distribution,

$$E\{\upsilon\} = 0, \qquad E\left\{\upsilon_j \upsilon_j^T\right\} = \sigma_j^2$$

- **Velocity Errors**

Input errors on the instrument inertial velocity are given along with error statistics by,

$$\vec{V}_{ECI}^{\,observed} = \vec{V}_{ECI}^{\,truth} + \varepsilon, \qquad E\{\varepsilon\} = 0, \qquad E\{\varepsilon_j \varepsilon_j^T\} = \sigma_j^2$$

The velocity affects the inertial pointing vectors $\hat{u}$ when accounting for aberration. The pointing vector with aberration correction can be simplified as,

$$\hat{p} = \frac{c\hat{u} + \vec{V}_{ECI}^T}{\left|c\hat{u} + \vec{V}_{ECI}^T\right|}, \qquad \hat{p} \approx \frac{c\hat{u} + \vec{V}_{ECI}^T}{c}, \qquad c \gg \left|\vec{V}_{ECI}^T\right|$$

We start again with the geolocation computation,

$$\vec{B}_{ECI} = \vec{X}_{ECI} + \rho \cdot \hat{p}$$

We form the geolocation errors as,

$$\Delta\vec{B}_{ECI} = \vec{B}_{ECI}^{\,observed} - \vec{B}_{ECI}^{\,truth} = \upsilon$$

$$\Delta\vec{B}_{ECI} \approx \left(\vec{X}_{ECI} + \rho \cdot \frac{c\hat{u} + \vec{V}_{ECI}^T + \varepsilon}{c}\right) - \left(\vec{X}_{ECI} + \rho \cdot \frac{c\hat{u} + \vec{V}_{ECI}^T}{c}\right)$$

Simplifying,

$$\Delta\vec{B}_{ECI} \approx \rho \cdot \frac{\varepsilon}{c} = \Delta t\, \varepsilon$$

where $\Delta t = \frac{\rho}{c}$

The resulting geolocation errors υ are scaled with respect to the velocity errors by the Δt term.

$$E\{\upsilon\} \approx 0, \qquad E\{\upsilon_j \upsilon_j^T\} \approx \sigma_j^2 \Delta t^2$$

Velocity is not necessarily an input used in the approximate geolocation algorithm. The inertial position of the instrument tracking point used in the approximate solution is an interpolated position at the ranging bounce point time. Velocity errors will manifest themselves as position errors if velocity is used in the interpolation or extrapolation computation. The elapsed time from transmit to the bounce point Δt is approximately 1.4 milli-seconds and given a conservative error estimate of 5 m/sec would produce geolocation errors of less than 1 cm. Therefore, these errors are expected to be very small and can be neglected.

- **Ranging Errors**

Input errors on the one-way transmit range leg are given by,

$$\rho^{observed} = \rho^{truth} + \varepsilon, \qquad E\{\varepsilon\} = 0, \qquad E\{\varepsilon\varepsilon^T\} = \sigma^2$$

We form the geolocation errors as,

$$\Delta\vec{B}_{ECI} = \vec{B}_{ECI}^{\,observed} - \vec{B}_{ECI}^{\,truth} = \upsilon$$

$$\Delta\vec{B}_{ECI} = \left(\vec{X}_{ECI} + \rho^{observed} \cdot \hat{p}\right) - \left(\vec{X}_{ECI} + \rho^{truth} \cdot \hat{p}\right)$$

$$\Delta\vec{B}_{ECI} = \varepsilon \cdot \hat{p}$$

The inertial pointing vector $\hat{p}$ provides the exact geolocation errors. If we assume the pointing is primarily along nadir the geolocation error expressed in the RIC frame simplify to,

$$E\{v\} \approx \begin{bmatrix}0\\0\\0\end{bmatrix}, \qquad E\{v_j v_j^T\} \approx \begin{bmatrix}\sigma^2\\0\\0\end{bmatrix}$$

- **Attitude Errors**

Let's define some useful quaternion notation first.

$$q = \begin{bmatrix}\varrho\\q_4\end{bmatrix}, \qquad \varrho = \begin{bmatrix}q_1\\q_2\\q_3\end{bmatrix} \equiv \sin\frac{\Delta\theta}{2}\begin{bmatrix}e_x\\e_y\\e_z\end{bmatrix}, \qquad q_4 \equiv \cos\frac{\Delta\theta}{2}$$

To transform from the observed or estimated state $q_{estimate}$, which is assumed to be close to the truth or true state q_{true}, one can define the rotation given by quaternion δq.

$$q_{true} = \delta q \otimes q_{estimate}$$

δq represents an error quaternion and is small. For small rotations,

$$\delta\varrho \approx \delta\alpha/2, \qquad \delta q_4 \approx 1$$

where $\delta\alpha$ has components of roll, pitch and yaw error angles $\begin{bmatrix}\phi\\\theta\\\psi\end{bmatrix}$ for any rotation sequence. Attitude errors are expressed as rotation angles from the δq error quaternion.

$$\begin{bmatrix}\phi\\\theta\\\psi\end{bmatrix} \approx 2\begin{bmatrix}\delta q_1\\\delta q_2\\\delta q_3\end{bmatrix}$$

These attitude errors express the uncertainty in the orientation of the optical bench frame (OBF) axes with respect to an inertial frame (ex. J2000) and impact the accuracy of the inertial pointing unit vector $\hat{\rho}$. A laser pointing vector in the optical bench frame $\hat{L}_{OBF}$ is computed, where the attitude errors are expressed.

The pointing vector estimate, $\hat{L}_{OBF}^{estimate}$ is computed using the true or known pointing vector, and applying roll, pitch and yaw error angle rotations,

$$\hat{L}_{OBF}^{estimate} = R'_{\phi} R'_{\theta} R'_{\psi} \hat{L}_{OBF}^{true}$$

The rotations matrices above are transposed because the attitude errors take us from the estimated state to the true state,

$$\hat{L}_{OBF}^{true} = R_{\psi} R_{\theta} R_{\phi} \hat{L}_{OBF}^{estimate}$$

Finally, the pointing is expressed in the inertial frame,

$$\hat{\rho} = R_{OBF \to ECI} \hat{L}_{OBF}^{estimate}$$

where it is used to compute the representative geolocation errors.

Using the known or true laser pointing unit vector of interest in the OBF frame $\hat{L}_{OBF}^{true}$, the errors are given as,

$$\Delta\vec{B}_{ECI} = \vec{B}_{ECI}^{\,observed} - \vec{B}_{ECI}^{\,truth} = v$$

$$\Delta\vec{B}_{ECI} = \left(\vec{X}_{ECI} + \rho \cdot \hat{p}^{observed}\right) - \left(\vec{X}_{ECI} + \rho \cdot \hat{p}^{truth}\right)$$

Expressed in the SBF frame,

$$\Delta\vec{B}_{OBF} = \rho\left(R'_{\phi}R'_{\theta}R'_{\psi}\hat{L}^{true}_{OBF} - \hat{L}^{true}_{OBF}\right) = \rho\left(R'_{\phi}R'_{\theta}R'_{\psi} - I\right)\hat{L}^{true}_{OBF}$$

And in the inertial frame,

$$\Delta\vec{B}_{ECI} = \rho R_{OBF\to ECI}\left(R'_{\phi}R'_{\theta}R'_{\psi} - I\right)\hat{L}^{true}_{OBF}$$

A simpler and generally accurate approach is to assume pointing near nadir, then the geolocation errors $\Delta\vec{B}_{OBF}$ are approximately,

$$\Delta\vec{B}_{OBF} \approx \rho\begin{bmatrix}\tan\theta\\ -\tan\phi\\ 0\end{bmatrix}$$

where and θ and ϕ are the pitch and roll error angles respectively. Yaw error angles introduce little to no error for nadir pointing beams. The geolocation errors can then be transformed into any frame of interest.

To summarize, the attitude errors are given as the δq error quaternion with statistical distributions given by,

$$\begin{bmatrix}\phi\\ \theta\\ \psi\end{bmatrix} \approx 2\begin{bmatrix}\delta q_1\\ \delta q_2\\ \delta q_3\end{bmatrix} = \varepsilon, \qquad E\{\varepsilon\} = \begin{bmatrix}0\\0\\0\end{bmatrix}, \qquad E\{\varepsilon\varepsilon^T\} = \begin{bmatrix}\sigma_\phi^2 & 0 & 0\\ 0 & \sigma_\theta^2 & 0\\ 0 & 0 & \sigma_\psi^2\end{bmatrix}$$

For nadir pointing and small rotations we arrive at,

$$\Delta\vec{B}_{OBF} \approx \rho\begin{bmatrix}\tan\theta\\ -\tan\phi\\ 0\end{bmatrix} \approx \rho\begin{bmatrix}\theta\\ -\phi\\ 0\end{bmatrix}, \text{for small rotations}$$

$$E\left\{\Delta\vec{B}_{OBF}\right\} \approx \begin{bmatrix}0\\0\\0\end{bmatrix}, \qquad E\left\{\Delta\vec{B}_{OBF}\Delta\vec{B}^T_{OBF}\right\} \approx \rho^2\begin{bmatrix}\sigma_\theta^2 & 0 & 0\\ 0 & \sigma_\phi^2 & 0\\ 0 & 0 & 0\end{bmatrix}$$

Or for an exact representation:

$$\Delta\vec{B}_{OBF} = \rho\left(R'_{\phi}R'_{\theta}R'_{\psi} - I\right)\hat{L}^{true}_{OBF}$$

Where the statistical mean $E\left\{\Delta\vec{B}_{OBF}\right\}$, and covariance matrix $E\left\{\Delta\vec{B}_{OBF}\Delta\vec{B}^T_{OBF}\right\}$ can be computed numerically.

- **Timing Errors**

Errors associated with the time tags of each input realize themselves as errors in the inputs themselves. For each input the partial derivative with respect to a change in time ∂t can be computed,

$$\left(\vec{X}_{ECI}, \hat{p}, \rho\right) \rightarrow \left(\frac{\partial \vec{X}_{ECI}}{\partial t}, \frac{\partial \hat{p}}{\partial t}, \frac{\partial \rho}{\partial t}\right)$$

The geolocation computation in the inertial frame:

$$\vec{B}_{ECI} = \vec{X}_{ECI} + \rho \cdot \hat{p}$$

Produces a change in ranging bounce point location $\Delta\vec{B}_{ECI}$ due to an error in reported time tag dt,

$$\Delta\vec{B}_{ECI} = \frac{\partial \vec{X}_{ECI}}{\partial t} dt + \frac{\partial \rho}{\partial t} dt \cdot \hat{p} + \rho \cdot \frac{\partial \hat{p}}{\partial t} dt$$

GEDI time tags are expected to be corrected within 50 ns of GPS time. Given a spacecraft velocity of 7600 m/sec, this would produce sub-mm geolocation errors. Attitude is practically constant over these time scales and would not introduce measurable differences from errors in pointing. Range errors are expected to include errors from inexact timing of the ranging observation and are different from the time tag errors introduced in this section. Therefore, time tags errors are ignored in this document.

- **Error Outputs for GEDI**

Input errors for the geolocation error analysis are provided in the ancillary input files. Table 3-3 shows the input error variables provided with 1σ uncertainty. The errors are transformed into corresponding 1σ geolocation error estimates that are listed in Table 3-3. The input errors are assumed to represent a Gaussian distribution with no mean value or biases. If these errors had any known or unknown biases the instrument calibration procedure would estimate the biases and eliminate their effect on the geolocation output. Other simplifications to this process include neglecting velocity and time tag errors due to their minimal impact on the geolocation output. Path delay errors are not included in this section, but Section 3.4 discusses how one would compute a change in bounce point coordinates for a change in atmospheric path delay.

Errors input and output estimates are also reported giving only the square root of the diagonal elements of the covariance matrix. This means that if there were to exist any strong cross-correlations between the inputs or output we would not be able to tell. The geolocation computation is done in an inertial frame, but the output uncertainty parameters are given in different reference frame coordinates. To get the outputs in geodetic coordinates it is necessary to transform the inertial geolocation position errors into ECF coordinates (as in Section 3.1, STEP 6), and then into ENU coordinates as in Section 3.3. Finally, the ENU coordinates are transformed into delta latitude $\Delta\phi$, delta longitude $\Delta\lambda$, and delta ellipsoid height Δh, as presented in Section 3.4.

Below, the procedure is given once geolocation inertial errors $\Delta\vec{B}_{ECI}$ are computed for reference ranging point i,

$$\Delta\vec{B}_{ECF}(i) = R_{ECI \rightarrow ECF}\left(t_B(i)\right) \Delta\vec{B}_{ECI}(i)$$

$$C_{ECF}^{ENU} = \begin{bmatrix} -sin\lambda & cos\lambda & 0 \\ -cos\lambda sin\phi & -sin\lambda sin\phi & cos\phi \\ cos\lambda cos\phi & sin\lambda cos\phi & sin\phi \end{bmatrix}$$

where ϕ and λ are the geodetic latitude and longitude (Section 3.2) of the reference ranging bounce point position.

$$\begin{bmatrix} \Delta u_e \\ \Delta u_n \\ \Delta u_{up} \end{bmatrix} = C_{ECF}^{ENU} \Delta \vec{B}_{ECF}(i)$$

Finally, the geodetic output errors in Table 3-3 are given,

$$\Delta\phi(i) = \frac{\Delta u_n}{R_E}, \qquad \Delta\lambda(i) = \frac{\Delta u_e}{R_E \cos\phi}$$
$$\Delta h(i) = \Delta u_{up}$$

Where geodetic latitude and longitude are converted into degrees.
To get corresponding along and cross-track (*sigma_along* and *sigma_across*) error components in Table 3-3,

$$\begin{bmatrix} \Delta u_{radial} \\ \Delta u_{intrack} \\ \Delta u_{cross} \end{bmatrix} = R_{ECI \to RIC} \Delta \vec{B}_{ECI}(i)$$
$$sigma\_along = \Delta u_{intrack}$$
$$sigma\_across = \Delta u_{cross}$$

- **GEDI implementation for reference ranging point *i*:**

This section uses the exact notation from Section 3's approximate algorithm formulation to compute inertial geolocation error estimates $\Delta \vec{B}_{ECI}(i)$ for reference ranging point *i*. The procedure discussed above is then followed to produce the output parameters of Table 3-3. The input errors are assumed to be zero-mean and be represented by the diagonal covariance matrix *P* of general form,

$$\varepsilon \sim N(0, P), \qquad P = \begin{bmatrix} \sigma_1^2 & 0 & 0 \\ 0 & \ddots & 0 \\ 0 & 0 & \sigma_N^2 \end{bmatrix}$$

where the uncertainty estimates σ_i are given for elements *i*. The uncertainty estimates must be interpolated to the reference ranging points transmit time, $t_T(i)$ to produce a geolocation error estimate.

- **Position**

  Inertial instrument position error uncertainty time histories $\delta \vec{X}_{ECI}^{\sigma}$ are provided in ANC02 and correspond directly to the provided instrument inertial positions.

$$\delta \vec{X}_{ECI}^{\sigma}(t_B(i)) = \begin{bmatrix} \sigma_x \\ \sigma_y \\ \sigma_z \end{bmatrix}, \qquad \Delta \vec{B}_{ECI}^{orbit}(i) = \begin{bmatrix} \sigma_x \\ \sigma_y \\ \sigma_z \end{bmatrix}$$

- **Ranging**

  One-way ranging error uncertainty time histories o^{σ} are provided in L1A. It is assumed that these range errors have timing inaccuracies incorporated into them.

$$\delta o^{\sigma}(t_T(i)) = \sigma\,, \qquad \Delta\vec{B}_{ECI}^{ranging}(i) = \sigma \cdot \hat{p}(t_T(i))$$

- **Pointing**

Pointing error uncertainty time histories δq_L^{σ} are provided in ANC03 and correspond directly to the provided pointing vectors in this file.

$$2\delta q_L^{\sigma} = 2\begin{bmatrix}\delta q_L^{\sigma}{}_1\\ \delta q_L^{\sigma}{}_2\\ \delta q_L^{\sigma}{}_3\end{bmatrix} = \begin{bmatrix}\sigma_\phi\\ \sigma_\theta\\ \sigma_\psi\end{bmatrix}$$

$$\Delta\vec{B}_{ECI}^{attitude}(i) = \rho R_{OBF\to ECI}\big(t_T(j)\big)\big(R'_\phi R'_\theta R'_\psi - I\big)\hat{p}$$

$$\hat{p} = R'_{OBF\to ECI}\big(t_T(i)\big)\hat{L}_{ECI}\big(t_T(i)\big)$$

$$R_\phi = \begin{bmatrix}1 & 0 & 0\\ 0 & \cos\sigma_\phi & \sin\sigma_\phi\\ 0 & -\sin\sigma_\phi & \cos\sigma_\phi\end{bmatrix}, \qquad R_\theta = \begin{bmatrix}\cos\sigma_\theta & 0 & -\sin\sigma_\theta\\ 0 & 1 & 0\\ \sin\sigma_\theta & 0 & \cos\sigma_\theta\end{bmatrix},$$

$$R_\psi = \begin{bmatrix}\cos\sigma_\psi & \sin\sigma_\psi & 0\\ -\sin\sigma_\psi & \cos\sigma_\psi & 0\\ 0 & 0 & 1\end{bmatrix}$$

- **Total Geolocation Error Estimate:**

All the individual error sources can be summed together to produce a total error estimate for reference ranging point *j*,

$$\Delta\vec{B}_{ECI}^{Total}(i) = \Delta\vec{B}_{ECI}^{orbit}(i) + \Delta\vec{B}_{ECI}^{ranging}(i) + \Delta\vec{B}_{ECI}^{attitude}(i)$$

Now the inertial error estimate can be transformed into geodetic, along and cross track coordinates as shown in the preceding section.

- **Height Scaling Factor**

For reference ranging points that noticeably differ in height from the reference ranging point the geolocation errors begin to deviate from the errors of the reference ranging point. A scaling factor is used to compute error estimates for all ranging points in the group. Orbit and ranging uncertainties affect every ranging point in the same way. However, ranging points can have range observations that vary noticeably in the group. Therefore, each ranging point one-way range accurately scales the errors of the reference ranging point in the group. So, the pointing error estimate is revisited again to scale the errors.

$$\Delta\vec{B}_{ECI}^{attitude}(i) = \rho R_{OBF\to ECI}\big(t_T(i)\big)\big(R'_\phi R'_\theta R'_\psi - I\big)\hat{p}$$

Next, the partial with respect to a change in measured range is,

$$\frac{\partial\Delta\vec{B}_{ECI}}{\partial\rho} = R_{OBF\to ECI}\big(t_T(i)\big)\big(R'_\phi R'_\theta R'_\psi - I\big)\hat{p}$$

And a new error estimate for the j^{th} ranging is simply,

$$\Delta\vec{B}_{ECI}(i) = \Delta\vec{B}_{ECI}(i) + \frac{\partial\Delta\vec{B}_{ECI}}{\partial\rho}(\rho(j) - \rho(i))$$

The procedure introduced above is then followed to transform the new errors into different components (geodetic and along/cross-track). It is important to note that this computation scales all components, not just height. Because pointing is primarily along nadir, the horizontal changes can be ignored without much consequence.

- **Summary**

A simulation with position, velocity, ranging and attitude error input histories was performed for ICESat-2 to compare predicted and computed geolocation errors. Geolocation errors were computed from the difference between true bounce point positions and estimated bounce points with the input errors. The true bounce point position came from using error free inputs and computing bounce points on the WGS-84 reference ellipsoid. The estimated bounce point came from using the true round-trip range observations and adding in errors to all the inputs including the range observations themselves. Both the rigorous and approximate algorithms themselves were tested to observe the error results. Predicted geolocation error estimates used the error histories on the inputs to analytically calculate a history of geolocation errors. The equations presented in this section were used to predict these errors. The figure bellows shows the numerically computed and analytically predicted geolocation errors in the RIC frame. The predicted errors lay on top of the numerically computed (truth) errors.

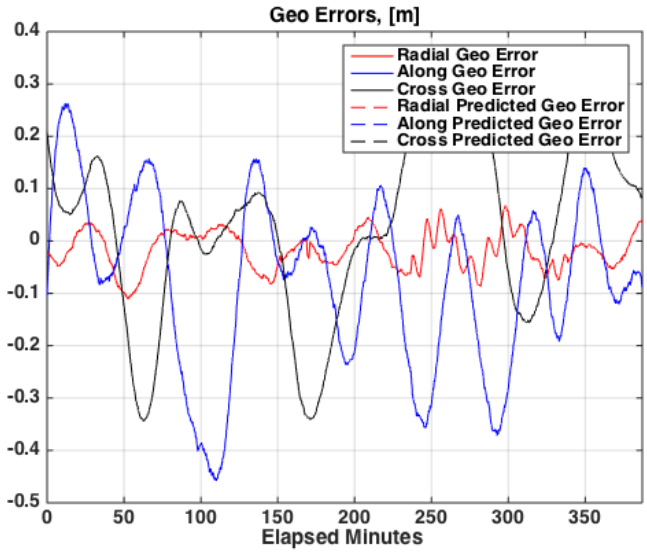

Figure 7 Simulated (computed) errors versus predicted geolocation errors

The next figure differences the predicted and computed errors from using the rigorous algorithm. The difference is many orders of magnitude below the geolocation errors themselves.

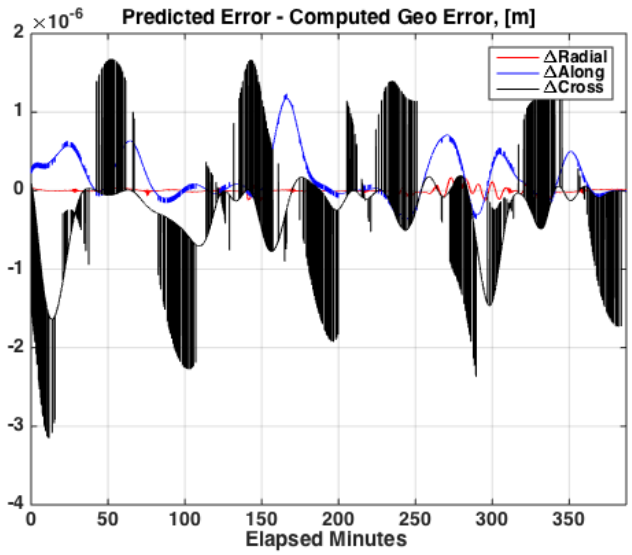

Figure 8 Difference between predicted and computed errors using rigorous geolocation

The next figure differences the predicted and computed errors from using the approximate algorithm. The difference is many orders of magnitude below the geolocation errors themselves. Notice that the radial prediction is about 0.016 cm off from the computed error. This is an artifact of using the approximate algorithm to perform the geolocation. The error is negligible.

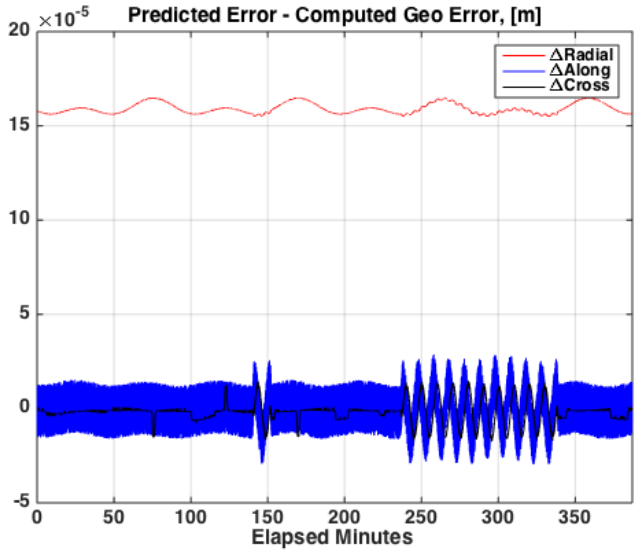

Figure 9 Difference between predicted and computed errors using approximate geolocation

The covariance matrix is shown for both the rigorous and approximate algorithms below. The predictions are very close to the computed error in both cases. The predictions do not vary because the formulas presented in this section do not change. The values used for bounce time, transmit range and other parameters are the approximated ones used in Section 3.1.

```
RIC Geolocation Error Covariance Matrix

      Computed [cm]                Predicted [cm]
 13.026  -17.249   5.586       13.026  -17.249   5.586
-17.249  275.207 -60.027      -17.249  275.207 -60.027
  5.586  -60.027 294.858        5.586  -60.027 294.858
```

Figure 10 Rigorous algorithm and predicted geolocation error covariance (Note units are cm^2 and not cm).

```
RIC Geolocation Error Covariance Matrix

      Computed [cm]                Predicted [cm]
 13.025  -17.251   5.587       13.026  -17.249   5.586
-17.251  275.207 -60.028      -17.249  275.208 -60.027
  5.587  -60.028 294.858        5.586  -60.027 294.858
```

Figure 11 Approximate algorithm and predicted geolocation error covariance (Note units are cm^2 and not cm).

Finally, below the approximate algorithm (with no input errors) differences with respect to the true bounce point are shown. Notice the 0.016 cm radial difference that appears in Figure 3-3 above.

```
Geolocation Error Statistics from Approx Algorithm
Radial Geolocation mean and stdev [cm] :  -0.016   0.000
Along  Geolocation mean and stdev [cm] :   0.000   0.001
Cross  Geolocation mean and stdev [cm] :   0.000   0.001
```

Figure 12 Approximate algorithm error statistics

Extensive testing through simulation has verified that the equations presented in this section produce accurate error estimates to sub-millimeter precision.

3.7 Geophysical Corrections

The models, algorithms and constants used in computing the geophysical corrections are documented in "ICESat-2 Project ATBD for Global Geolocated Photons, ATL03, Section 6.0 Geophysical Corrections".

The following list summarizes time-dependent geophysical corrections and static reference values required to produce the geolocated waveforms in the L1 and L2 products and provided in the /geophys_corr data group within the L1 and L2 data products. This list is similar to corrections and standards applied in other altimetric and geodetic satellite missions, as well as multi-national climatological investigations (e.g., ESA's Sea Level Climate Change Initiative).

The following parameters are located in the /geophys_corr data group of the L1 and L2 products. **The ellipsoid height of bounce points within the /geolocation group (*elevation_bin0* and *elevation_lastbin*) have been corrected for solid earth tides, ocean loading, solid earth pole tide, and ocean pole tide.** The bounce points are NOT corrected for ocean tides and dynamic atmospheric correction. These corrections are applied by subtracting the corrections from the

bounce point elevations. To remove the corrections already applied (restore the geophysical signal of interest) one needs to add the corrections to the bounce point elevations.

- **Ocean Tides** including diurnal and semi-diurnal (harmonic analysis), and longer period tides (dynamic and self-consistent equilibrium) (±5 m)
- **Dynamic Atmospheric Correction** (DAC) including **inverted barometer** (IB) effect (±5 cm)
- **Solid Earth Tides** (±40 cm, max)
- **Ocean Loading** (-6 to 0 cm)
- **Solid Earth Pole Tide** Deformation due to centrifugal effect from small variations in polar motion (±1.5 cm)
- **Ocean Pole Tide** Oceanic height correction due to centrifugal effect from small variations in polar motion (±2 mm amplitude)
- **Geocenter Motion** correction *not* applied to L2 science products, but is accounted for in precision orbit determination. (amplitude 3 to 5 mm in X,Y,Z).

Photon round-trip range corrections:

- **Total column atmospheric delay** (-2.6 to -0.9 m)

Static and Quasi-static parameters (reference values):

- **Geoid** (-105 to +90 m, max)
- **Mean Sea Surface** (-105 to +87 m)

4.0 PRECISE POSITIONING

4.1 Overview

The purpose of Precise Positioning is to determine the locations of the GEDI instrument transmit and receive points, which are necessary for geolocation of the laser altimeter ranging points. To accomplish this, Precise Positioning first computes the location of the ISS center of mass in the J2000 frame, then a constant vector offset (fixed in the OBF frame) from the ISS center of mass to the GEDI instrument transmit and receive points is applied.

The GEDI payload will be flown onboard the International Space Station (ISS), located specifically at Exposed Facility Unit 6 (EFU-6) of the Japanese Experiment Module (JEM). Signal obstruction issues and expected motion of the GEDI GPS receiver antenna reference point (ARP) relative to the ISS center of mass at this location requires GEDI Precise Positioning to use alternative methods other than a standard precision orbit determination procedure.

First, reduced dynamic solutions for the ISS center of mass location will be computed using data from both the on-board GEDI GPS receiver and the ISS Space Integrated GPS/INS (SIGI) GPS receiver, as well as other GPS tracking data of opportunity from other GPS receivers on the ISS (Luthcke et al. 2003, Rowlands et al. 1997). Second, kinematic solutions for the position of the GEDI GPS receiver ARP will be computed using the reduced-dynamic solution as an a priori solution, where there is enough tracking data from the GEDI GPS receiver to support kinematic positioning. A constant vector offset (assumed constant in an ISS body-fixed frame) will be estimated from a pre-launch a priori CAD models and used to obtain the position of the ISS center of mass relative to the GEDI GPS receiver ARP.

Precise Positioning is responsible for producing the following ancillary data products to be used as inputs to the GEDI waveform geolocation:

Table 4-1 ANC Products Output by Precise Positioning

ANC Product	Description	Comments
ANC03	Precise Positioning ECI to ECF Quaternions	ECI Frame = J2000; ECF Frame = ITRF2014
ANC04	Precise Positioning Ephemeris	Ephemeris of ISS center of mass in J2000 ECI frame

4.2 Requirements

The requirement applicable to Precise Positioning is provided in the GEDI Geolocation Budget document (GEDI-SYS-REQ-0004E_Release_8-31-2016.xlsm). This requirement is provided in the table below:

Table 4-2 Requirements for Precise Positioning

Requirement	Value	Details
GPS position requirement	1.3 meters	This is the horizontal (RSS of along-track & cross-track) position requirement. This implies a radial position knowledge of < 25 cm.

4.3 Core Software

Precise Positioning will generate both reduced-dynamic and kinematic solutions. The reduced-dynamic solutions for the ISS center of mass will be generated using the GEODYN software package. The kinematic solutions for the GEDI GPS receiver ARP will be generated using the Interferometric Translocation (IT) software. These two primary software packages are described further in the following sections.

4.3.1 GEODYN

The software program used to compute the reduced-dynamic solutions for the ISS center of mass location is the GEODYN-II program, which evolved from the original GEODYN program that was developed at NASA GSFC in the 1960's. This current version of the software has been operational since 1985, and has been extensively used for satellite orbit determination, altimeter geolocation, geodetic parameter estimation, tracking instrument calibration, and orbit prediction, and is capable of handling essentially all types of satellite tracking data.

GEODYN-II has been utilized on every NASA geodetic Earth and planetary altimeter mission including TOPEX/Poseidon, JASON-1, JASON-2, Mars Global Surveyor, Shuttle Laser Altimeter I & II, GEDI, GRACE, Lunar Reconnaissance Orbiter, MESSENGER, and GRAIL. Of note is the use of the GEODYN-II program to achieve and confirm 1-centimeter radial orbit accuracy for JASON1 [Luthcke et al., 2003].

The orbit parameter and estimation problem is divided into two parts: (1) the orbit modeling or prediction problem, and (2) the parameter estimation problem. The solution to the first corresponds to GEODYN's orbit generation mode, which relies on Cowell's method of numerically integrating the orbit. The second part of the problem corresponds to GEODYN's data reduction mode, which is based on the solution to the orbit prediction problem, and utilizes Bayesian least squares statistical estimation procedure to optimally estimate the parameters. A brief overview of the GEODYN estimation and orbit modeling processes are provided in the appendix. For a more complete discussion of the GEODYN parameter estimation and orbit and measurement modeling algorithms please refer to [Pavlis et al., 1998].

4.3.2 Interferometric Translocation

Interferometric Translocation (IT) is a geodetic "GPS-only" navigation and surveying software package. It has been continuously developed by Oscar L. Colombo since 1991.

4.4 Implementation

This section provides an overview of the GEDI Precise Positioning implementation. It first provides the locations on ISS of the various components whose data is used to generate the positioning solutions. It then provides a comprehensive list of the data files and the constants, models, and standards used.

4.4.1 Component Locations

Precise Positioning will utilize data from both the GEDI and ISS (SIGI) GPS receivers. The image below from a Configuration Analysis Modeling and Mass Properties (CAMMP) analysis (CAMMP_Analysis_-_GEDI_GPS_-_EC-2553.pdf) shows the relative locations of the GEDI GPS receiver antenna and the four (4) ISS (SIGI) GPS receiver antennas. The analysis also provided estimates of these antenna locations relative to the SSACS (Section 1.4).

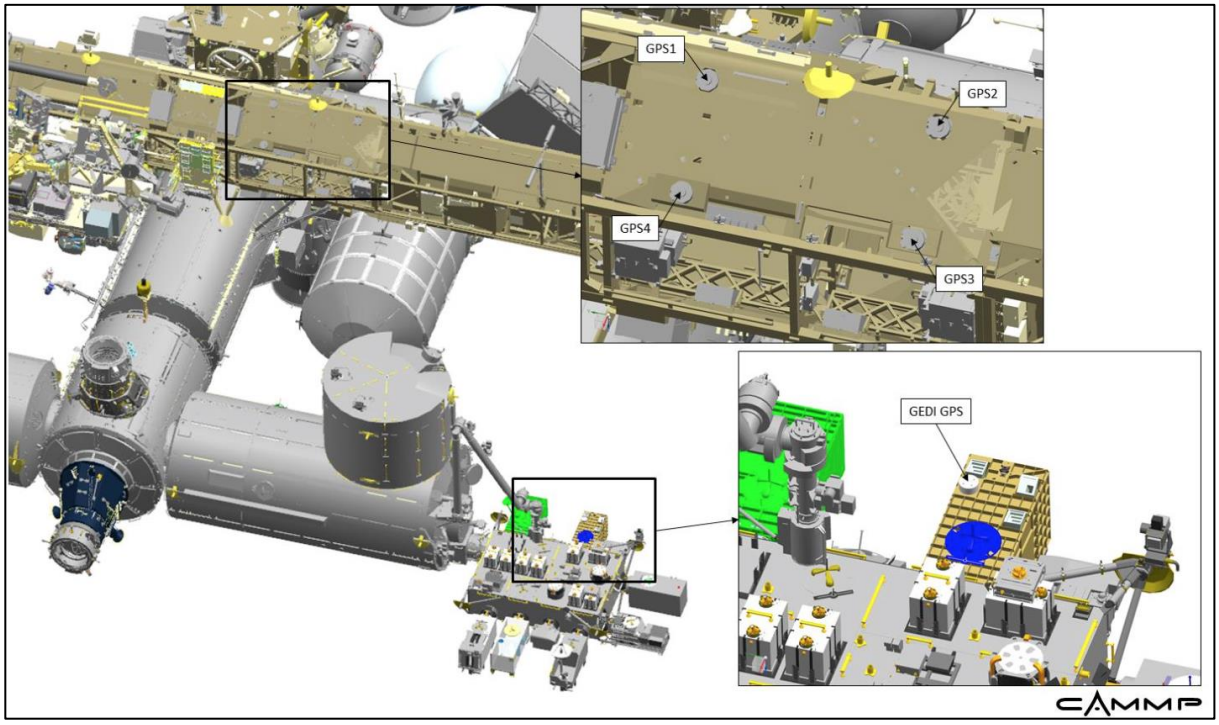

Figure 13 GEDI and ISS (SIGI) GPS Receiver Antenna Locations

Another CAMMP analysis estimated the ISS center of gravity location relative to the SSACS (EC-2581.pdf). The analysis considered an ISS configuration with the Russian Segment Node (RSN), which is planned for arrival in June 2018 prior to GEDI on SpX-18 planned for late 2018. Also considered was an ISS configuration with the Russian Segment Science and Power Module (SPM) installed on RSN port, which may arrive during GEDI operations. Both configurations evaluated visiting vehicle traffic on both the USOS docking/berthing ports and RS docking ports to provide the estimated center of gravity range.

The table below summarizes the results from the two CAMMP analyses, giving the locations of all relevant GPS receiver antennas and the estimated ISS center of gravity range. All locations are relative to the SSACS frame.

Table 4-3 Precise Positioning A Priori Component Locations (in SSACS frame)

Component	X (m)	Y (m)	Z (m)
GEDI GPS Receiver			
GEDI GPS Receiver Antenna	8.6449	-16.1828	6.4549
ISS (SIGI) GPS Receivers			
GPS1 Antenna	0.3002	-2.5723	-2.0655
GPS2 Antenna	0.3002	-5.6203	-2.0655
GPS3 Antenna	1.4559	-5.6203	-1.1824
GPS4 Antenna	1.4559	-2.5723	-1.1824
ISS Center of Gravity			
ISS with RSN	-4.38 to -2.78	-0.70 to -0.68	3.82 to 4.08
ISS with SPM	-4.88 to -3.60	-1.10 to -1.05	4.25 to 4.63

4.4.2 Input Data:

Precise Positioning will receive input data from two sources:
1. The Mission Operations Center (MOC)
2. The Geodetic Data Pre-Processing System (GDPS)

The inputs from each of these sources are described in detail in the following sections.

4.4.2.1 Input Data from the MOC:

The table below describes the Precise Positioning inputs obtained from the MOC. The formats of these files are defined in the MOC to SOC ICD (GEDI-GS-ICD-0029).

Table 4-4 Precise Positioning Data from MOC

GEDI GPS Receiver Data Files				
Description	File Name	Frequency	Latency	Comments
GEDI GPS LZP Files	GEDI_B_GPS_*YYYYDDDHHMMSS_YYYYDDDHHMMSS_vnn.tlm*	Daily	Nominally 3 hours	Raw GPS code and carrier phase observables GPS receiver NAV solution
ISS Data Files				
Description	File Name	Frequency	Latency	Comments
ISS Ancillary Data Files	ISS State: - ISS_Body_State - ISS_CoM_J2K_State - ISS_GPS_Nav_Soln Center of Mass: - MassInfo Attitude: - J2K2CTRS - J2K2BodyAtt Macro-Model: - BetaAngleBiases - RadiatorAngles	Daily	~2 Days	ISS C.O.M., position, velocity, attitude, center of mass

	- SolarArrayAngles - SolarLOS			

4.4.2.2 Input Data from GDPS:

The table below describes the Precise Positioning inputs obtained from GDPS:

Table 4-5 Precise Positioning Data from GDPS

GNSS Satellite Broadcast Ephemeris				
Description	File Name	Frequency	Latency	Comments
GPS satellite broadcast ephemeris	brdc*DoY*0.*YY*n	Daily	17-41 hours	Duplicate data blocks removed
GNSS Satellite Unhealthy Periods				
Description	File Name	Frequency	Latency	Comments
Unhealthy GPS satellite tables	unhealthy_gps_sats_*wwwwd*.tbl	Daily	17-41 hours	Unhealthy periods from broadcast ephemeris files
GNSS Satellite Orbits & Clock Corrections				
Description	File Name	Frequency	Latency	Comments
GPS satellite orbits	igs*wwwwd*.sp3	Daily	12-18 days	IGS final product
GPS satellite clock corrections	igs*wwwwd*.clk	Daily	12-18 days	IGS final product
GNSS Satellite Additional Information				
Description	File Name	Frequency	Latency	Comments
SVNPRN	svnprn_*wwww*	As necessary	N/A	The "wwww" number is associated with the igsyy_wwww.atx file from which it was created
GPS satellite summary	gps_satellite_summary_*wwww*.tbl	As necessary	N/A	
GPS satellite antenna PCV	gps_satellite_pcv_*wwww*.corr	As necessary	N/A	
IGS Tracking Station Data				
Description	File Name	Frequency	Latency	Comments
IGS tracking station RINEX observation files	*SITEDoY*0.*YY*o	Daily	As uploaded by stations	Original FixClock'd GPS satellite clock corrected
IGS Tracking Station Information				
Description	File Name	Frequency	Latency	Comments
IGS station summary tables	*center_wwww*_gps_station…_weekly_summary.tbl	Weekly	11-17 days	
IGS station antenna correction tables	*center_wwww*_gps_station…_annenna_correction.tbl	Weekly	11-17 days	
IGS station antenna lists	*center_wwww*_gps_station…_antenna_list	Weekly	11-17 days	
IGS station PCV corrections	*center_wwww*_gps_station…_pcv.corr	Weekly	11-17 days	

4.4.3 Observables, Models, Constants, Standards

4.4.3.1 GEDI-specific models & observables:

Table 4-6 GEDI-Specific Models & Observables

GEDI Specific Force Models		
Description	Model	Comment
Non-conservative force model	Panel model developed based on ISS geometry and surface optical properties. Tuned on orbit for the radiative force model component. Geometry used for drag computations.	
GEDI Specific Measurement Models		
Description	Model	Comment
GEDI GPS receiver antenna phase center offset vector and phase center variation map	Pre-launch measurements and tuned on-orbit	
Center of mass vector	Pre-launch model from CAAMP analysis. Receive as telemetered ancillary ISS data	
ISS attitude	Provided as telemetered ancillary ISS data	
GEDI attitude	Telemetered star tracker data	
GPS Tracking Data Observables		
Description	Model	Comment
Preprocessing	Conversion to RINEX-II/III format, FixClock, cycle slip detection and removal, bad GPS satellite detection and removal	Conversion from receiver code and carrier phase observables to calibrated RINEX standard pseudorange and carrier phase observations. FixClock used to estimate receiver clock offset.
Basic Observable	Ionosphere-free carrier phase and pseudorange observables. Corrected for 1st order by forming ionosphere-free linear combination.	
Modeled observables	Primary: double-differenced carrier phase with ionosphere-free linear combination applied. Secondary: single- and un-differenced observables	

4.4.3.2 GPS satellite force and measurement models:

Table 4-7 GPS Satellite Force and Measurement Models

GPS Satellite Force Models		
Description	Model	Comment
Non-conservative force model	Solar radiation pressure model: Adjustable box-wing model (TUMSOL) Earth shadow model: conic model with oblate Earth, umbra and penumbra Earth albedo: Standard model Attitude model: See GPS attitude model in GPS satellite measurement model section below	[Rodriguez-Solano, 2012] [Rodriguez-Solano, 2009] [Kouba, 2009]
GPS Satellite Measurement Models		

Description	Model	Comment
GPS satellite center of mass correction	Phase center offsets	
GPS satellite antenna phase center variations	PCV model with respect to phase center (elevation and azimuth dependent corrections)	
GPS satellite attitude model	GPS satellite yaw attitude for nominal periods Yaw-attitude model for eclipse periods, applied based upon nominal yaw rates Reverse-kinematic solution to provide alternative yaw-attitude solution during eclipse periods when Kouba's model may be inaccurate	[Bar-Sever, 1996] [Kouba, 2009; Kouba, 2013]
RHC phase rotation correction	Phase center wind-up	[Wu et al., 1993]
GPS satellite clock corrections	For un-differenced and single-differenced observables	IGS clock correction files (igswwwwd.clk)
GPS satellite relativistic clock corrections	For un-differenced and single-differenced observables	Computed and applied
GPS Ground Station Measurement Models		
Description	Model	Comment
GPS ground station network	40 IGS tracking stations, based upon station performance and geographic coverage. Positions and velocities are from IGS SINEX solution files	IGS SINEX
GPS ground station marker to antenna reference point (ARP) eccentricity	dN, dE, dU eccentricities applied	IGS SINEX
GPS ground station antenna phase center variations and corrections	PCV model applied Receiver antenna and radome types	igsyy_wwww.atx IGS SINEX
Atmospheric Path Delay (Troposphere)	General approach: Line-of-sight delay expressed as a function of four zenith delay parameters & scaling mapping functions. The four parameters are: hydrostatic zenith delay (computed), wet zenith delay, and N and E horizontal gradients. The mapping functions are: hydrostatic, wet, and gradient. Alternative approach: GEOD-FPIT model Wet scale parameters estimated ~hourly and gradient scale parameters estimated ~daily	IERS 2010 Chen and Herring (1997) gradient mapping function. VMF1 hydrostatic and wet mapping function (Boehn et al. 2006a) as primary. [Petrov] GMF hydrostatic and wet mapping function (Boehm et al., 2006b) as secondary.
Ionosphere Delay	1st order effect: removed by LC combination. For single frequency data: characterized. Higher order dispersive effects may be modeled	IERS 2010
Gravitational Delay	Gravitational delay due to Earth modeled	IERS 2010 (Eq. 11.17)

4.4.3.3 General Precise Positioning Models, Constants, and Standards:

Table 4-8 General Precise Positioning Models, Constants, and Standards

General Force Models		
Description	Model	Comment

Earth Reference Ellipsoid	a_e = 6378136.3 m 1/f = 298.2564	Semi-major axis value consistent with static gravity file being used Flattening value consistent with zero-tide definition (required by GEODYN)
Speed of Light	c = 299792458 m/s	
Geopotential	Static gravity file: *eigen-6c.gfc_20080101_do_200_fix.grv* GM = 398600.4415 km^3/m^2	Consistent with EIGEN-6C. To be updated as necessary. Epoch reset to the date of the projected mission center using only the trend components
Time variable gravity	ATGRAV file: *ATGRAV.glo-3HR_20160101-PRESENT_9999_AOD1B_0006.0090* Contribution from atmosphere, non-tidal oceans, hydrology, and ice.	[Luthcke et al., 2013]
Tidal	Solid Earth tide: IERS 2010 Ocean tide model: GOT4.10	IERS 2010 [Ray, 1999]
Solid Earth and Ocean Pole Tide: The centrifugal effect of polar motion	$\Delta\bar{C}_{2,1} and\ \Delta\bar{S}_{2,1}$ corrections Correction is a function of wobble parameters (m_1, m_2) which are related to the polar motion variables (x_p, y_p)	IERS 2010
N-body	Sun, Moon, all planets	JPL DE421
Atmospheric Drag	MSIS for atmospheric density	[Hedin, 1987]
Earth Albedo	Modeled	[Knocke et al., 1988]
Relativistic corrections	Schwarzschild term (acceleration due to point mass of Earth) – secular drift in argument of perigee Lense-Thirring and de Sitter terms (geodetic precession) – precession of the orbit plane	IERS 2010
Numerical Integration	Cowell predictor-corrector Fixed and variable step Equations of motion and variational equations	GEODYN implementation
Estimation Method	Partitioned Bayesian least squares	GEODYN implementation
General Reference Frame and Constants		
Description	Model	Comment
Time System	GPS time given by GEDI GPS receiver 1PPS and corrected based on position solutions	
Conventional Inertial System	J2000 S.I. units	IERS 2010
Precession / Nutation	IAU 2000A Precession-Nutation Model	[Coppola et al., 2009]
Planetary Ephemerides	JPL DE421	[Standish et al., 1995]
Earth Orientation Parameter (EOP) Model	IERS 08 C 04 IERS 2010 conventions for diurnal, semidiurnal, and long period tidal effects on polar motion and UT1	IERS 2010
UT1-TAI	IERS 08 C 04	IERS 2010
Terrestrial reference Frame	ITRF2014 reference frame realized through the set of station coordinates and velocities used as well as IGS GPS satellite orbits	
Ellipsoid	GEODYN: Consistent with geopotential	In GEODYN, flattening is used only to calculate rectangular coordinates for the tracking stations when geodetic coordinates are given, in defining the sub-satellite location for altimeter data, and in calculating the

		geodetic altitude for drag purposes
High-resolution Geoid	EGM2008 mean tide system	WGS-84 referenced
Land Topography	GMTED2010 30 arcsec	
Ocean Mean Sea Surface Topography	DTU15	

5.0 PRECISE POINTING DETERMINATION

5.1 Precise Pointing Overview

The purpose of Precise Pointing is to determine the inertial attitude of the GEDI instrument and the laser pointing vectors, which is necessary for geolocation of the GEDI ranging points. Precise Pointing will use data from three Danish Technical University (DTU) star trackers (μASC - micro Advance Stellar Compasses). Each star tracker or camera head unit (CHU) comes with an integrated MEMS micro inertial reference unit (mIRU). Each star tracker will provide the following data:

- Inertial to star tracker frame attitude solutions
- 4 dual-axis accelerometer measurements from mIRU
- Three-axis gyroscope angular rate measurements from mIRU

The final attitude solution used for onboard processing is computed from utilizing attitude solutions from all three star trackers and using the high rate mIRU data to propagate the attitude. The ground-processing algorithms and procedures are discussed in more detail in the next section.

Precise Pointing is responsible for producing the following ancillary data products to be used as inputs to the GEDI waveform geolocation:

Table 5-1 ANC Products output by Precise Pointing

ANC Product	Description	Comments
ANC05	PPD Vectors and Quaternions File	Beam pointing unit vectors in inertial frame Inertial to OBF attitude quaternions Inertial Frame = J2000

5.2 Requirements

The requirement applicable to Precise Positioning was discussed in Section 1.4, *Geolocation knowledge budget*.

Table 5-1 Budget for Precise Pointing

Budget	Value	Details
Attitude Solution	2.4”	This is the intended accuracy of the attitude solution of the OBF.

The pointing budget accounts for additional errors (jitter, misalignment, etc.) that get added (RSS) to the attitude error. The systematic components of the total pointing error are expected to be compensated for through instrument calibration employing range residual analyses. This process is further discussed in Section 6.0, *GEOLOCATION PARAMETER CALIBRATION Overview*.

5.3 Precise Pointing Implementation

5.3.1 Ground Post-Processing

Precise ground attitude determination implements a Multiplicative Extended Kalman Filter (MEKF). A specific star tracker camera head unit (CHU) is defined as the attitude determination frame (ADF). The CHU's optical measurements are used as the filter's observations and the fused (gyro and accelerometer measurements) angular rates from the ADF CHU's mIRU are used to propagate the estimated ADF attitude forward. A Rauch-Tung-Striebel (RTS) backwards filter is applied afterward which is the equivalent of a batch filter for dynamic systems.

The filter states include attitude corrections (3) to the ADF attitude reference, angular rate bias estimates (3) which are applied to the angular rate data, and relative alignment states (9) to the other two CHUs and a synthetic star tracker created from ISS attitude measurements. The relative alignment estimates allow for the optical measurements from the other sources to be included as additional observations in the filter and are intended to improve the solution through blinding intervals. More details concerning the filter formulation can be found in ICESat-2's PPD ATBD (ICESat-2-SIPS-SPEC-1595.pdf). Additional equations and details can be found in the book *Optimal Estimation of Dynamic Systems, by John L. Crassidis and John L. Junkins, Section 7.1 Attitude Estimation*.

Due to the restricted field of view and harsh lighting environment on the ISS, all trackers are often blinded (3 heads within 30 deg separation), and when not blinded have bright reflections (solar panels, etc.) that can degrade the attitude solution. This challenge lead to the integration of ISS attitude solutions that are utilized as additional measurements in the attitude filter.

5.3.2 Input Data from the MOC:

Precise Pointing will receive input data from the Mission Operations Center (MOC). The inputs are described in detail below. The formats of these files are defined in the MOC to SOC ICD (GEDI-GS-ICD-0029).

Table 5-2 Precise Positioning Data from the MOC

GEDI Housekeeping Data Files				
Description	File Name	Frequency	Latency	Comments
GEDI Tracker and PCS housekeeping file	GEDI00_B_STFUSED-CHU*_*YYYYDDDHHMMSS_YYYYDDDHHMMSS* _v*nn*.csv GEDI00_B_PLATATT_*YYYYDDDHHMMSS_YYYYDDDHHMMSS* _v*nn*.csv GEDI00_B_PCS-*_*YYYYDDDHHMMSS_YYYYDDDHHMMSS* _v*nn*.csv	Daily	Nominally 3 hours	Star tracker and PCS data
ISS Data Files				
Description	File Name	Frequency	Latency	Comments
ISS Ancillary Data Files	Attitude: - J2K2CTRS - J2K2BodyAtt	Daily	~2 Days	ISS attitude solutions

5.4 Precise Pointing Outputs

The following list contains Precise Positioning outputs:

- ANC05 ancillary product file
- $R_{ECI \rightarrow OBF}$, J2000 to OBF rotation
- L_{ECI}, GEDI beam unit vectors in the inertial frame (J2000)

5.5 Reference Documents

- GE-DTU-ICD-3004 v0_91 TMTC ICD – DRAFT
- ICESat-2-SIPS-SPEC-1595.pdf
- Optimal Estimation of Dynamic Systems, by John L. Crassidis and John L. Junkins
- GEDI-GS-ICD-0029

6.0 GEOLOCATION PARAMETER CALIBRATION OVERVIEW

Laser pointing, ranging, timing and orbit errors must be compensated in order to accurately geolocate the laser altimeter surface returns. The returned waveform ranging observations can be exploited in an integrated residual analysis to accurately calibrate these geolocation/instrument parameters [Luthcke et al. 2000, 2002, 2005]. For GEDI, as with LVIS, SLA-1&2, and ICESat-1, we apply this approach, processing GEDI altimeter range observations from ocean scans (OS) and "round"-the-world scans (RTWS) along with dynamic crossovers in order to calibrate and correct the systematic pointing and ranging errors (SP&RE) in the form of biases, trends and orbital variation parameters [Luthcke et al. 2005].

OS and RTWS are specifically designed calibrations that use commanded GEDI pointing maneuvers and ocean altimeter range observations to recover pointing, ranging and timing parameters [Luthcke et al. 2000]. The parameters are estimated from a batch reduction of the altimeter range residuals using Bayesian least-squares differential corrections. For GEDI, the maneuver is deliberate instrument roll deviation from nominal reference ground track pointing, while the pitch variation comes from the dead-band wobble about nadir of the ISS attitude. Each 20 minute OS has two complete periods around the local nadir direction. The RTWS calibration maneuvers are simply OS maneuvers performed continuously over oceans for 1.5 orbit revolutions (performed for the tracks with the most ocean coverage). Detailed error analysis and application show these maneuvers are a strong filter for isolating systematic pointing errors from other systematic error sources such as ranging errors [Luthcke et al. 2000 and 2002].

For GEDI, the OS maneuvers will be performed nominally twice per day over the mid-Pacific: one to be done approximately at orbit noon and one approximately at orbit midnight to capture any instrument thermal-mechanical variation. Pointing biases in both the OBF Coordinate Systems X and Y axes, along with a range bias, are estimated through the reduction of the ocean surface altimeter range residuals from each OS. The RTWS calibrations are performed nominally every eight-days during the orbit track that has the most ocean coverage, and provide a means to estimate remaining SPE orbital variation as a function of orbit angle (angle between the satellite position vector and the sun vector projected in the orbit plane where 0° is orbit 6AM and 90° is orbit noon). Through the reduction of the range residuals from the RTWS, pointing biases in both the OBF X and Y axes are nominally estimated every 7.7 minutes or every 30° in orbit angle. The resulting OS and RTWS calibration history facilitate sub-arcsecond calibration of SPE (orientation and amplitude) at time scales of ~8-minutes to months [Luthcke et al. 2002, 2005].

7.0 REFERENCES

- Coppola, V. T., Seago, J. H., Vallado, D. A., "The IAU 2000a and IAU 2006 Precession-nutation Theories and Their Implementation." *American Astronautical Society*. 2009.

- Guinot, B., "Report of the Sub-group on Time", in *Reference Systems*, J. A. Hughes, C. A. Smith, and G. H. Kaplan (eds.), U. S. Naval Observatory, Washington, D. C., 3-16, 1991.

- Hofmann-Wellenhof, B., H. Lichtenegger, and J. Collins, *GPS: Theory and Practice*, Third Edition, Springer-Verlag, Wien, 1994.

- Luthcke, S.B., D.D. Rowlands, J.J. McCarthy, E. Stoneking and D.E. Pavlis, Spaceborne Laser Altimeter Pointing Bias Calibration From Range Residual Analysis, Journal of Spacecraft and Rockets, Vol. 37, No. 3, May-June, pp. 374-384, 2000.

- Luthcke, S.B., C.C. Carabajal and D.D. Rowlands, Enhanced geolocation of spaceborne laser altimeter surface returns: parameter calibration from the simultaneious reduction of altimeter range and navigation tracking data," Journal of Geodynamics, Vol. 34, No. 3-4, October/November, pp. 447-475, 2002.

- Luthcke, S.B., N.P. Zelensky, D.D. Rowlands, F.G. Lemoine and T.A. Williams, The 1-centimeter Orbit: Jason-1 Precision Orbit Determination Using GPS, SLR, DORIS and Altimeter data, *Marine Geodesy,* Special Issue on Jason-1 Calibration/Validation, Part 1, Vol. 26, No. 3-4, pp. 399-421, 2003.

- Luthcke, S.B., D.D. Rowlands, T.A. Williams, M. Sirota,"Reduction of ICESat systematic geolocation errors and the impact on ice sheet elevation change detection," Geophys. Res. Lett., 32, L21S05, doi:10.1029/2005GL023689, 2005.

- McCarthy, D. D., *IERS Technical Note 21*, July 1996.

- Petit, G. and B. Luzum, 2010, "IERS Conventions (2010)," IERS Technical Note No. 36, International Earth Rotation and Reference System Service (IERS).

- Rowlands, D.D., Luthcke, S.B., Marshall, J.A., Cox, C.M., Williamson, R.G. and Rowton, S.C., "Space Shuttle Precision Orbit Determination in Support of SLA-1 Using TDRSS and GPS Tracking Data," Journal of Astronautical Sciences, Vol. 45, No. 1, January-March 1997, pp. 113-129, 1997.

- Standish, E. M., Newhall X X, Williams, J. G. and Folkner, W. F., 1995, "JPL Planetary and Lunar Ephemerides, DE403/LE403", JPL IOM 314.10-127, 1995.

- Smith, N., Bae, S., Schutz, B., "Algorithm Theoretical Basis Document for Precision Pointing Determination, ICESat-2-SIPS-SPEC-1595.pdf", Texas Center of Space Research, 2015

- Crassidis, J.L., Junkins, J.L. “Optimal Estimation of Dynamic Systems”, Second Edition, 2012.

GLOSSARY/ACRONYMS

ASAS	ATLAS Science Algorithm Software
ATBD	Algorithm Theoretical Basis Document
ATLAS	Advance Topographic Laser Altimeter System
CAMMPS	Configuration Analysis Modeling and Mass Properties
CHU	Camera Head Unit
CoM	Center of Mass
DPU	Data Processing Unit
DTU	Danish Technical University
ECF	Earth Centered Fixed
ECI	Earth Centered Inertial
FOV	Field Of View
GED	GEDI Coordinate System (GEDI Frame)
GEDI	Global Ecosystem Dynamics Investigation
GPS	Global Positioning System
ICRS	International Celestial Reference System
IERS	International Earth Rotation Service
ISS	International Space Station
ITRF	International Terrestrial Reference Frame
JD	Julian Date
JPL	NASA Jet Propulsion Lab
LF	Laser Frame
MIRU	Micro Inertial Reference Unit
µASC	Micro Advanced Stellar Compass
mIRU	Micro Inertial Reference Unit
MIS	Management Information System
MJD	Modified Julian Date
MOC	Mission Operations Center
N	Nutation
OBF	Optical Bench Frame
POD	Precision Orbit Determination
P	Precession
PCS	Pointing Control System ???
PPD	Precision Pointing Determination
PSO	Project Science Office
R	Earth’s spin
RGT	Repeat Ground Track
RMS	Root Mean Squared

RSS	Root Sum Squared
SBF	Spacecraft Body Fixed
S/C	Spacecraft
SCoRe	Signature Controlled Request
SDMS	Scheduling and Data Management System
SF	Star Frame
SIPS	Science Investigator-led Processing System
SSACS	Space Station Analysis Coordinate System
TAI	International Atomic Time
TBD	To Be Determined
TDT	Terrestrial Dynamic Time
TT	Terrestrial Time
USNO	United States Naval Observatory
UTC	Coordinated Universal Time
W	Polar motion
ZRP	Zero Range Point